Recent thermohaline shifts in the Adriatic Sea and their potential consequences

Elena Terzić[1] and Ivica Vilibić[1,2]

[1]Ruđer Bošković Institute, Division for Marine and Environmental Research, Bijenička cesta 54, 10000 Zagreb, Croatia
[2]Institute for Adriatic Crops and Karst Reclamation, Put Duilova 11, 21000 Split, Croatia

Correspondence: Elena Terzić (eterzic@irb.hr)

Abstract. The Adriatic Sea has warmed and salinified rapidly over the past two decades, and the changes are not uniform with depth. We combine 34 306 quality-controlled shipboard temperature and salinity casts spanning 1950–2025, from which two climatologies are built, adding Argo float data in the Southern Adriatic Pit, to quantify the vertical structure of the change and to test formally for eventual regime changes. Between the 1950–1999 and 2000–2025 climatologies the southern Adriatic warmed and salinified at every depth and season, by 0.10–0.52 in salinity and up to 1.6 °C in temperature. Amplification relative to the Mediterranean is strongly depth-dependent, reaching 6.1-fold for temperature below 700 m while remaining below the basin median above 200 m. Near-surface salinity maxima ("surface saline lakes") become about four times more frequent after 2014, representing a regime shift that is demonstrable only once vertical resolution is controlled for. The double salinity maximum structure is modified as well: the intermediate maximum has lost the dominant band of the classical description, and where two maxima coexist they move apart and diverge in density, so they are not one migrating core. Over 2014–2024 the steric contribution in the Southern Adriatic Pit is negative, dominated by halosteric contraction, so that local sea level rise must be mass-driven. Salt fingering has intensified below the double salinity maximum structure, allowing for salt transport towards deeper layers.

Three consequences follow, set out here as hypotheses. Deep ventilation may persist under milder winters, because water that is already saline needs less cooling to sink, yet deliver less oxygen per event because the water that sinks is warmer. Exchange of oxygen, nutrients and carbon between the surface and intermediate layers may be either suppressed or enhanced beneath more frequent surface saline lakes, depending on whether stratification or double diffusion prevails. Adriatic ecosystems, in which warming-linked mortality and species redistribution are already documented, face a basin changing faster at depth than at the surface. Testing these requires sustained high-resolution observation.

1 Introduction

Coastal and marginal seas respond to climate forcing faster than the open ocean, whether the forcing arrives from the atmosphere, from land, or across lateral boundaries (Holt et al., 2025; Richardson et al., 2025; Wagawa and Igeta, 2025). The Mediterranean Sea is the archetype, changing at rates above the global ocean mean (Schroeder et al., 2017; Juza et al., 2022),

and within it the Adriatic Sea is a particularly sensitive sub-basin: semi-enclosed, 800 km long, 200 km wide and up to 1230 m deep, strongly influenced by riverine input, and subject to orographically shaped air–sea forcing.

Four Adriatic processes are directly relevant here. North Adriatic Dense Water (NAddW) forms on the shallow northern shelf and cascades along the bottom into the Jabuka and Southern Adriatic Pits, bringing oxygen to the deep layers (Zore-Armanda, 1963; Marini et al., 2006; Vilibić et al., 2023). The inflow of saline Levantine and Cretan Intermediate Water (LIW/CIW) is modulated on decadal scales by the Adriatic–Ionian Bimodal Oscillating System (Gačić et al., 2010; Civitarese et al., 2023), shaping the thermohaline properties and the nutrient budget of the basin (Civitarese et al., 2010). The Eastern Mediterranean Transient of the early 1990s, when the Aegean replaced the Adriatic as the dominant source of eastern Mediterranean deep water (Roether et al., 1996), is the precedent for an abrupt reorganisation on this scale, and it altered Adriatic properties directly (Vilibić et al., 2012). Open-ocean convection in the Southern Adriatic Pit supplies deep water to the Eastern Mediterranean (Gačić et al., 2002; Schlitzer et al., 1991). The small internal Rossby radius of the Adriatic makes its dynamics fast and spatially fine-grained (Cushman-Roisin and Korotenko, 2007; Pranić et al., 2023).

Since the early 2010s these processes appear to have moved outside their historical envelope. Salinity rose sharply after 2017 (Mihanović et al., 2021; Beg Paklar et al., 2020), dense waters formed in 2017, 2018 and 2022 were produced by weak cooling of very saline water rather than by strong cooling (Terzić et al., 2025a; Amorim et al., 2024; Le Meur et al., 2025), and near-surface salinity maxima were documented for the first time (Terzić et al., 2025b). Whether these are genuinely abrupt departures, or the visible part of a gradual trend sampled by a rapidly improving observing system, has not been tested formally. That distinction is important because the observing system changed at almost exactly the time the signal appeared: Argo entered the Adriatic in 2009 and now dominates the deep observations (Tintoré et al., 2019).

Three developments make a quantitative reassessment timely. The Adriatic in situ record has been consolidated across archives, so historical shipborne casts and modern autonomous profiles can be processed through a single pipeline. Argo now provides more than a decade of deep profiling in the Southern Adriatic Pit, enough to resolve the vertical structure of the change rather than only its surface expression. The same pipeline can also be applied to every Mediterranean sub-basin, which turns the recurring claim of local amplification from a qualitative impression into a testable ratio.

This research article is organised as follows. Section 2 describes the observational dataset and the methods. Section 3 addresses four questions: how large are the Adriatic changes, and are they distinguishable from sampling variability (Sects. 3.1–3.2)? Is the amplification relative to the Mediterranean general, or confined to particular depths (Sect. 3.3)? Did the vertical distribution of salinity in the intermediate layer change over time (Sect. 3.4)? Is the increase in near-surface salinity maxima (surface saline lakes) an abrupt shift or an artefact of vertical resolution (Sect. 3.5)? Sections 3.6–3.7 quantify the steric and double-diffusive consequences. Section 4 discusses the implications as hypotheses and identifies the observations and model experiments that would test them.

2 Data and methods

2.1 Observational dataset

Climatologies are built from all quality-controlled in situ temperature and salinity casts available in the Adriatic for 1950–1999 and 2000–2025. Three archives are combined. The SeaDataNet Pan-European infrastructure supplies the Mediterranean aggregated dataset SDC_MED_DATA_TS_V2 (Simoncelli et al., 2020), which archives observations from 1912 to 2019, retrieved in December 2025. Local Adriatic databases are contributed by the Institute of Oceanography and Fisheries (Adriatic database 1987–2019, and the Palagruža Sill transect 1952–2018) and the Ruđer Bošković Institute (northern Adriatic transect 1979–2018), together with the Croatian MSFD monitoring CTD set (2019–2023). Argo profiles come from Euro-Argo ERIC, accessed through `argopy` (Maze and Balem, 2020) and retrieved in January 2026; the first Adriatic profile dates from 2009. The Adriatic casts used here are the Adriatic subset of the Mediterranean-wide multiplatform dataset assembled and described by Terzić and Vilibić (2026c), processed through the same chain, so the Adriatic and Mediterranean sides of the comparison in Sect. 2.4 rest on one dataset rather than on two independently curated ones. The cleaned Adriatic in situ files are archived by Terzić and Vilibić (2026a) and the processing and analysis code by Terzić and Vilibić (2026b).

Table 1 reports retained cast counts by source, region, period, season and maximum depth. These are the counts entering Figs. 1–2, not the raw archive totals. Quality control follows the originating infrastructure: SeaDataNet procedures (SeaDataNet, 2010) and Argo delayed-mode procedures (Wong et al., 2023), with only flags 1 and 2 accepted in both. Casts from national and international cruises outside those archives were quality controlled following SeaDataNet procedures during the assessment described by Pranić et al. (2023). Duplicates are removed by matching position, time and platform before pooling, so a cast archived in more than one source is counted once.

All analyses use the record to 2025. The climatological comparison — Figs. 1, 2 and 4 and Tables 1 and 2 — contrasts 1950–1999 with 2000–2025, and the 34 306 casts of Table 1 are drawn from those two windows.

The two periods are not sampled alike. Argo supplies 44.3 % of the 21st-century southern Adriatic casts and none of the 20th-century ones, and Argo profiles do not reach the top few metres – their median first sampled depth in the southern Adriatic is 5.5 m, against 2.8 m for the 21st-century casts of all platforms together – so the shallowest bins are the least comparable between periods (Sect. 3.1).

2.2 Regions, binning and climatologies

The northern and southern Adriatic are delimited by two polygons, labelled DJ1 and DJ3 after the Mediterranean sub-basin nomenclature of Manca et al. (2004). The labels follow that nomenclature but the boundaries do not: rather than straight lines of latitude, they follow the coastline and the bathymetry, so that the northern shelf is separated from the middle Adriatic along the Zadar–Ancona axis rather than across it, and the southern Adriatic is separated from the middle along the Gargano–Pelješac axis. Bounding boxes are given in Table 1 and the polygon files are archived with the analysis code. Seasons are three-month bins, JFM, AMJ, JAS and OND. Casts are binned onto 22 standard levels between 5 and 1200 m. A cast contributes to a level only where it carries a finite, flag-1 or flag-2 value; no vertical interpolation across gaps is performed, and casts that do not

reach the full depth simply stop contributing below their deepest level. A level is retained when at least 5 % of the casts in that region, period and season reach it. Averaging is by measurement within each level, and a second pass rejects values more than one standard deviation from the first-pass bin mean.

Temperature and salinity are binned as measured, that is as in situ temperature and practical salinity; practical salinity is a ratio and is therefore reported without units. Potential density anomaly referenced to the surface (σ_0) is derived from them through TEOS-10 (IOC et al., 2010), which converts practical salinity to absolute salinity and in situ to conservative temperature internally, using the `gsw` implementation. The Argo-based analyses of Sects. 2.7 and 2.8 work directly in absolute salinity and conservative temperature, since they require the thermodynamic coefficients. The binning and pooling procedure is described in more detail by Terzić and Vilibić (2026c), who apply it Mediterranean-wide.

2.3 Uncertainty of climatological differences

Counting casts as independent measurements would overstate how much information the climatologies contain. A research cruise typically occupies a region for a few days and takes many casts in that time, so those casts largely repeat one synoptic state rather than sampling the climate independently: 200 casts from four cruises carry far less information than 200 casts taken on 200 separate occasions.

The uncertainty is therefore estimated by bootstrapping. No values are simulated and no distribution is assumed: each of the 2000 replicate datasets is built only from observations already in the archive, drawn at random with replacement, so a given cast may appear several times in one replicate and not at all in another. The period mean is recomputed on each replicate, and the confidence interval is the spread of those 2000 means. The wider they scatter, the less the single observed mean can be relied on.

The resampling unit is the cruise-day rather than the cast: all casts taken by one cruise on one day enter or leave a replicate together, so the replicates inherit the repetition of the real sampling. The ratio between the variance obtained this way and the variance obtained by treating casts as independent is the variance inflation factor, which is at least one, so clustering always widens the interval: a value of 6 means the casts carry the information of about one sixth as many independent observations. For 2000–2025 it is 1.8–2.2 in the southern Adriatic and 5.7–6.3 in the northern Adriatic (for 1950–1999, when sampling was still more cruise-bound, 3.8–5.7 and 7.0–8.3, respectively), so the northern shelf, where cruises are denser and more repetitive, is far more strongly clustered. Shaded envelopes in Figs. 1–2 are 95 % confidence intervals on the period mean at each level, computed this way; they are not standard deviations.

Northern Adriatic results are reported only to 50 m, because below that depth the region is barely sampled: 905 casts reach beyond 50 m in 2000–2025 against 12 697 above it, over 90 % of those stop between 50 and 75 m, and fewer than 30 reach 100 m in either period (Table 1), so the 50–200 m row of that table describes a layer that is in practice 50–75 m thick.

2.4 Adriatic–Mediterranean rate comparison

To make the amplification claim quantitative, deseasoned linear trends per decade are computed for every Mediterranean sub-basin with the same pipeline, bins, quality control and estimator as for the Adriatic, so that the only difference between the

two sides of the comparison is the ocean rather than the method. The monthly basin-by-depth series and the seasonal-harmonic trend model are those of Terzić and Vilibić (2026c), re-fitted here over the matched window. Mediterranean values are the median across basins outside the Adriatic with the interquartile range; Adriatic values are the median across depth bins within a layer. The Adriatic sub-basins are excluded from the reference median so that the basin is not compared partly against itself; including them changes no ratio qualitatively (the largest effect is on surface salinity, 4.3 to 3.6). The four layers – 5–50, 75–200, 250–600 and 700–1200 m – separate the seasonally mixed surface layer, the layer between the seasonal thermocline and the LIW/CIW horizon, the intermediate-water core, and the deep layers renewed episodically by cascading. The conclusions do not depend on these boundaries, since any partition of the standard levels gives a temperature ratio below one above 200 m and above four below 700 m. The window is 2000–2025, matching the climatologies; the resulting sampling asymmetry is quantified in Sect. 2.1.

2.5 Change-point analysis

Whether the change in the occurrence of surface saline lakes (SSLs) is a step rather than a gradual drift is tested with the rank-based Pettitt (1979) test. The test tries every possible break year in turn, measures how different the years before it are from the years after it, and keeps the year that separates them best. Because it searches the years itself, the result is not biased by our picking a year by eye.

Its p-value is obtained by simulation rather than from the standard formula, which assumes each year is independent of the last. We generate 5000 artificial series that match the observed mean, variance and year-to-year correlation but contain no change point by construction, run the identical test on each, and report the fraction that produce a step at least as large as the observed one. Years with fewer than 20 casts are dropped.

Detection of an SSL depends strongly on vertical resolution (Sect. 3.5), so the test is run on a resolution-matched subset: casts with median level spacing ≤ 5 m and at least 8 levels in 0–100 m. The justification is a direct degradation experiment, in which Argo profiles are re-sampled onto progressively coarser grids and the identical detection is repeated (Fig. A1).

2.6 Detection of surface saline lakes

Detection uses raw profiles rather than the binned climatologies of Sect. 2.2, so the cast set is assembled separately and is larger: 11 106 southern Adriatic casts over 1950–2025. Occurrence is shown from 1985 because nothing earlier can be evaluated: of the 313 casts from 1950–1984 whose vertical resolution can be computed, not one meets the resolution criteria of Sect. 2.5. The reason is not spacing alone. The threshold itself requires 5 m spacing, but even against a looser 10 m criterion no cast before 1975 qualifies; the late 1970s are better sampled than that suggests – 68 % of the 1975–1979 casts meet 10 m and 12 % meet 5 m – and those finer casts fail instead on level count, carrying only three or four levels in the upper 100 m against the eight the detection requires (Fig. A1).

Following Terzić et al. (2025b), a cast is recorded as an SSL when all four of the following hold, with salinity throughout taken as practical salinity and its gradient therefore in m^{-1}: (i) the vertical salinity gradient falls below $-0.01\ \mathrm{m}^{-1}$ somewhere in 0–100 m, defining a halocline core, chosen among candidates as the one nearest 100 m; (ii) the maximum salinity gradient

above the core stays below 0.02 m^{-1}, so the feature is not simply the lower flank of a shallower feature; (iii) the surface is at least 0.05 saltier than the core; and (iv) the water column above the core is statically stable in density, verified with a stratification index computed across the halocline with a 5 m vertical offset, so the salinity inversion is temperature-compensated rather than convectively unstable. Casts with fewer than 8 finite levels in the 0–100 m window are not evaluated.

2.7 Detection of double salinity maxima

The intermediate salinity structure is characterised by locating every prominent subsurface maximum in each cast rather than a single core depth, so that a cast carrying two maxima is described by two, and any change in their separation is measurable. Maxima are found by peak prominence in salinity, the prominence of a peak being the drop in salinity from it to the lowest point that must be crossed to reach any higher peak. The threshold is 0.010. It is set from the data: in casts that carry two maxima the weaker of the two stands 0.021 in salinity above the minimum separating it from the stronger (Sect. 3.4), so a threshold at about half that value admits the real second maximum while rejecting smaller wiggles. It is varied between 0.005 and 0.030 in the sensitivity test of Appendix A (Fig. A3). The search runs to 900 m and requires at least 8 levels in it, a floor that sets aside 469 of the 5761 southern Adriatic casts (8.2 %) as too coarse to carry the detection. The upper 20 m are excluded, so that the near-surface maximum of a surface saline lake is not counted as an intermediate core.

Within each cast, only the two most prominent maxima are retained; no cast is excluded. This guards against a small number of very finely resolved historical profiles whose fine structure is instrumental noise rather than signal: they return up to 268 nominal maxima each, and uncapped, 20 such casts would supply 56 % of all 1950–1999 detections. The cap falls on a similar share of casts in each period, 47 % against 46 %, so it does not favour either. Prominence ranks the maxima because it measures how far a peak stands above the profile around it, and so how much of a distinct feature rather than a ripple it is.

Both choices, together with the prominence threshold itself and the depth a cast must reach, are free parameters, so the whole analysis is repeated across a grid of them in Appendix A (Fig. A3). Both quantities the paper draws conclusions from – how strongly the maxima concentrate in the historical 100–200 m band, and the contrast between how the two members changed in density – hold in every configuration tested.

Each maximum carries its depth, salinity, temperature and σ_0. The σ_0 is what separates the two ways a maximum can move: if it changes depth but keeps its density, the water has simply been displaced; if its density changes as well, the water itself is different. The search runs to 900 m, but frequency statistics use only casts reaching 700 m, since a shallower cast cannot be counted as lacking a deep maximum it could not have seen. Detection runs on the profiles at their native vertical resolution; because that resolution improves over the record, the whole detection is repeated on modern profiles degraded to historical standard depths, and both results are reported in Sect. 3.4. The two periods compared are 1950–1999 and 2000–2025, as for the climatologies.

2.8 Steric decomposition

Thermosteric and halosteric height are computed from ascending Argo profiles reaching at least 1000 dbar in the Southern Adriatic Pit, following Wang et al. (2017), as

$$\mathrm{TSLA} = \int \alpha\,\Theta'\,\mathrm{d}z, \qquad \mathrm{HSLA} = -\int \beta\,S'_{\mathrm{A}}\,\mathrm{d}z, \tag{1}$$

where primes denote anomalies about the period-mean profile and α, β are the TEOS-10 thermal expansion and haline contraction coefficients. The anomaly form is required rather than merely preferred: integrating $\alpha\Theta$ instead of $\alpha\Theta'$ makes the result, and its trend, depend on the temperature scale used, because Θ is measured from an arbitrary origin while α varies with depth. Anomalies remove that origin.

Profiles are interpolated onto a common 0–1000 dbar grid at 5 dbar spacing, the shallowest observation being carried to the surface since Argo does not sample the top few metres (median first sampled depth 5.5 m for the southern Adriatic floats). Monthly means are formed and the annual and semi-annual harmonics removed, and trends are least-squares fits.

Two features of the series govern how it is treated. First, successive months are correlated, so the record carries less information than its 121 monthly values suggest; the confidence intervals therefore rest on an effective sample size, reduced in proportion to the lag-one correlation of the residuals (Bretherton et al., 1999). That correlation is 0.7–0.8, leaving an effective 10–21 independent values, so the intervals are correspondingly wide. Second, the thermosteric and halosteric components move in opposition, and much of what makes each uncertain affects both in the same way and cancels in their sum. Adding two separately fitted trends would discard that cancellation and inflate the uncertainty on the net, so the net is formed profile by profile and trended once. Seventeen floats contribute 694 profiles over April 2010 – September 2025; WMO identifiers are listed in Table 4. Two further floats, 6903805 and 6901865, are excluded because their profiles do not reach 1000 dbar in the Southern Adriatic Pit.

2.9 Double-diffusive diagnostics

Two quantities are distinguished. The Turner angle determines whether the column is in the salt-finger regime ($45^\circ \le \mathrm{Tu} < 90^\circ$); the density ratio R_ρ determines whether fingering there is dynamically effective. They are computed from vertical gradients of conservative temperature and absolute salinity as

$$\mathrm{Tu} = \arctan\frac{\alpha\,\partial_z\Theta - \beta\,\partial_z S_{\mathrm{A}}}{\alpha\,\partial_z\Theta + \beta\,\partial_z S_{\mathrm{A}}}, \qquad R_\rho = \frac{\alpha\,\partial_z\Theta}{\beta\,\partial_z S_{\mathrm{A}}}, \tag{2}$$

with the four-quadrant arctangent, alongside the squared buoyancy frequency $N^2 = -(g/\rho)\,\partial\rho/\partial z$, which measures how strongly the column is stratified. All are evaluated with the `gsw` implementation of TEOS-10 (IOC et al., 2010). Fingers transport appreciably for $R_\rho < 2$, marginally to about 4, and negligibly beyond about 10 (Schmitt, 1994), because they transport salt only if they reach full amplitude before internal-wave shear disrupts them, and the time they need to grow is set by R_ρ (Kunze, 1987). A column can therefore be entirely finger-favourable by the Turner angle and still transport nothing, so extent and vigour are reported separately. Both use the same 694 Argo profiles as the steric decomposition, a Southern Adriatic Pit set

retrieved separately in September 2025, and, like it, need vertical gradients resolved over a few metres through the full column and repeated through the year; only Argo provides that here, so neither can be extended into the shipborne record.

They are evaluated in three layers, because the layers behave differently and averaging across them cancels their changes out. The layers are the ones used throughout: 200–400 m, the classical range of the LIW salinity maximum (Artegiani et al., 1997) and the range within which our detected maxima sit (Sect. 3.4); 400–600 m, into which the deeper maximum has descended; and 600–1000 m, the deep layer. A fourth, 350–550 m, is computed only for comparison with the EMSO-E2M3A mooring in Sect. 4.2 and carries no result here. Profiles are compared before and from 2017 with a two-sided Mann–Whitney test on the per-profile layer statistics.

3 Results

3.1 Southern Adriatic warming and salinification

Between the 1950–1999 and 2000–2025 climatologies the southern Adriatic (DJ3) is warmer and saltier at every depth from 5 to 1200 m and in every season (Fig. 1). Salinity differences range from $+0.098$ to $+0.522$ and are distinguishable from sampling variability at all 88 depth–season combinations after cruise-day clustering is accounted for. Temperature differences range from -1.22 to $+1.56\,^{\circ}\mathrm{C}$ and are significant at 97 % of combinations. The summer of 1950–1999 is the thinnest cell of the whole design, 444 casts against 1852 in 2000–2025 (Table 1), so the summer differences carry the widest intervals and are the ones most exposed to the sampling change discussed next.

The most negative of those differences, $-1.22\,^{\circ}\mathrm{C}$ in the 5 m summer bin, is an artefact of how the surface is sampled rather than a cooling. In summer 1950–1999, 82 % of southern Adriatic casts began at or above 1 m and the median first sample was at the surface; over 2000–2025 only 20 % do, the median first sample is at 2.5 m, and Argo – which supplies most recent profiles – has a median summer first sample at 5.8 m. Binning does not remove this bias, because recent casts enter the shallowest bin only through its deeper, colder part. Against the 20th-century summer thermocline of $0.34\,^{\circ}\mathrm{C\,m^{-1}}$ over the top 20 m, a first sample at 2.5 m instead of the surface reads about $0.8\,^{\circ}\mathrm{C}$ too cold and one at 5.8 m about $2.0\,^{\circ}\mathrm{C}$ too cold, so the observed $-1.22\,^{\circ}\mathrm{C}$ lies between these values. We therefore do not interpret the uppermost summer bin, and read the 5–10 m levels with the same caution. Below 30 m, where the profile is smooth and the platforms overlap, the differences are positive at every level and season. Below 200 m the warming is 0.4–0.6 °C and quasi-uniform across seasons (Fig. 1, bottom row).

Potential density has the weaker signal: 64 % of depth–season combinations show a significant difference, because thermal and haline effects oppose one another. Below 600 m they compensate almost exactly, which is the physical statement behind the near-zero deep steric trend in Sect. 3.6.

3.2 Northern Adriatic shelf

In the northern Adriatic (DJ1, Fig. 2, 0–50 m) warming reaches 3.0 °C at 20 m in summer, and surface salinity increases in every season, by $+0.09$ to $+0.18$ in winter, spring and autumn but by $+1.00$ in summer, so the seasonal contrast between the

fresh summer surface and the winter state is much reduced (Fig. 2). The evidence is weaker than in the south, and unevenly so: once clustering is accounted for, 88 % of the depth–season combinations reported here are significant for temperature but only 71 % for salinity. The northern shelf is where the clustering correction is largest, with variance inflation factors of 5.7–6.3, and it is also where 20th-century sampling is concentrated along the western coastline while salinity is systematically higher along the eastern one (Artegiani et al., 1997; Vilibić et al., 2019). The 21st-century casts sit farther east and north than the 20th-century ones (median cast longitude 13.7°E against 13.1°E), on the saltier side of that gradient, so the spatial sampling shift inflates rather than damps the apparent salinification. Northern Adriatic salinity differences should therefore be read as indicative upper bounds rather than established values, and we do not report DJ1 below 50 m at all (Sect. 2.3).

3.3 The amplification is depth-dependent

On matched periods and an identical pipeline (Table 2), the southern Adriatic exceeds the Mediterranean basin median by a factor of 6.1 for temperature and 3.8 for salinity at 700–1200 m. Above 200 m the temperature ratio is 0.5–0.7: the southern Adriatic warms more slowly than the Mediterranean median in the upper layers. Amplification is therefore not a single number: a single figure for the basin would average a sixfold deep signal against an upper-layer deficit and obscure both.

The ratio is one of rates fitted within the 2000–2025 window (Sect. 2.4), not of the climatological differences shown in Figs. 1–2. The platform change still acts inside that window, since Argo's share grows through the 2000s and Argo does not reach the 5 m bin. Excluding the shallowest bins therefore tests the ratio directly: restricting the surface layer to 10–50, 20–50 and 30–50 m moves the temperature ratio from 0.55 to 0.38, 0.37 and 0.35, and the salinity ratio from 4.3 to 4.1, 3.7 and 3.7. The upper-layer temperature deficit is thus robust, and if anything understated. The deficit is also consistent with the large climatological differences of Fig. 1: the Mediterranean median itself warms at 0.41 °C per decade in the surface layer, so a southern Adriatic surface rate of 0.22 °C per decade is a below-median rate even though the difference it accumulates between 1950–1999 and 2000–2025 is large. Ranked against all 28 sub-basins on this pipeline, the southern Adriatic is the sixth slowest-warming at 5–50 m, placing it in the bottom quartile; the northern Adriatic, by contrast, is the fifth fastest. The upper Adriatic is therefore not uniformly slow either – the deficit is specific to the southern basin.

Salinity behaves differently from temperature. The salinity ratio is 4.3 at 5–50 m, 1.3 at 75–200 m, 1.9 at 250–600 m and 3.8 at 700–1200 m, so haline amplification is present through the whole column, with a minimum at intermediate depths. Only the thermal amplification is deep-specific: the southern Adriatic is salinifying faster than the Mediterranean median everywhere, but warming faster than it only below 200 m. These ratios are window-mean rates, which is what the climatological difference in Figs. 1–2 measures, and are not the acceleration of those rates. Terzić and Vilibić (2026c), on the same dataset, find Mediterranean warming and salinification to be accelerating rather than linear, with the acceleration peaking in the Adriatic–Ionian sector; a quadratic fit to the series used here reproduces that, giving the southern Adriatic $+0.29$ per decade^2 in surface salinity. A basin whose rate was modest early in the window and high late in it has an unremarkable window-mean rate but a large acceleration, so the two statements are compatible.

The deep-layer ratios are the robust part of this comparison; the shallow ones should be read together with the sampling caveats above.

3.4 The intermediate salinity maximum has lost its dominant band

The classical description of the southern Adriatic intermediate layer is of a single salinity maximum, associated with the inflow of Levantine Intermediate Water and typically found between 200 and 400 m (Artegiani et al., 1997). We test that description directly by detecting every prominent salinity maximum in each cast rather than one core depth (Sect. 2.7), and asking where those maxima sit.

The change is in where the maxima lie rather than in how many there are. Two maxima are not a modern feature: among casts deep enough to resolve both, 65.8 % carried two in 1950–1999 and 68.6 % in 2000–2025. This is the one quantity in this section that depends on the detection settings: across the grid of Appendix A it rises significantly in some configurations and falls significantly in others, so we draw no conclusion from it beyond the absence of a consistent trend. What did change is their concentration. In 1950–1999 the detections cluster in one band: 28 % of them fall in a single 50 m interval at 100–150 m and 42 % within 100–200 m. This band is where the detections themselves concentrate and is not a definition of the core; it spans the shallower member and the top of the classical 200–400 m range. In 2000–2025 that same band holds only 16 %, and the detections spread through the column in both directions – 43 % now lie above 100 m against 26 % before, and 30 % below 300 m against 17 % (Fig. 4). The historical profile therefore had a dominant intermediate maximum, which a single-core description represents adequately; the modern one does not.

The two features have also moved apart. Measured within each cast, the median separation between them grew from 92 m in 1950–1999 to 113 m in 2000–2025 ($p = 6 \times 10^{-7}$, Mann–Whitney), and the spread of separations grew far more, from an interquartile range of 31–160 m to one of 29–378 m: some casts now carry two maxima very close together and others two that are hundreds of metres apart. Pooled across casts, the deeper member sits at a median 325 m (95 % confidence interval 295–345 m) against 201 m (183–228 m) before, and the shallower at 78 m (75–81 m) against 100 m (86–111 m); the intervals do not overlap for either member. These pooled medians describe the two populations and are not the separation within a cast, which is why they do not subtract to it. Their densities diverged with their depths: the shallower maximum became 0.12 kg m^{-3} lighter as it salinified, while the deeper one changed by only 0.03 kg m^{-3} and so stayed close to its isopycnal. A feature that is simultaneously saltier and markedly lighter cannot be the same water displaced upward, so the two are not one migrating core.

They have not, however, become sharper. The salinity drop from the weaker maximum to the minimum between the two, which measures how distinctly the pair stands apart, is unchanged: a median of 0.021 in both periods, with overlapping confidence intervals (0.017–0.032 and 0.020–0.023). The maxima are therefore differently placed rather than better resolved.

Two checks support this. Repeating the detection on modern profiles degraded to historical standard depths gives 44.0 % of detections in the 100–200 m band for 1950–1999 against 15.0 % for 2000–2025, against 41.7 % and 15.5 % at native resolution, so the contrast is not an effect of the finer modern sampling. The concentration in that band is higher in 1950–1999 than in 2000–2025 under every combination of the detection parameters we tested, as is the excess lightening of the shallow member over the deep one (Fig. A3).

3.5 Surface saline lakes: an abrupt shift

Detection rates differ by a factor of 25 between platforms in the Fig. 3 cast set: 0.58 % for SeaDataNet, 3.75 % for the IOR database, 12.14 % for MSFD CTD and 14.87 % for Argo. In 2017 alone, SeaDataNet found one SSL in 37 southern Adriatic casts while Argo found 89 in 191, in the same basin and year. The degradation experiment identifies the cause (Fig. A1): re-sampling Argo profiles onto coarser grids reduces detections from 438 at native 1–5 m spacing to 434 at 2 m, 244 at 5 m, 52 at 10 m and zero on the standard bottle grid (0, 10, 20, 30, 50, 75, 100 m). At bottle resolution the criterion detects nothing, even in profiles that demonstrably contain a surface saline lake, because it requires a salinity gradient steeper than $-0.01\,\mathrm{m}^{-1}$ across a feature a few metres thick. The near-zero historical occurrence is therefore partly instrumental, and Fig. 3 is built on resolution-matched casts.

The resolution threshold retains 5244 of the 7202 casts for which vertical resolution could be computed. Enough historical data meets it: SeaDataNet holds substantial high-resolution CTD in the southern Adriatic, with a median level spacing of 1 m, so 75 of the 171 casts in 1985–1989 and 1188 of the 1543 casts in 1990–1999 satisfy the spacing and level-count criteria, against 2269 of 2270 in 2016–2025 (Table 1). SeaDataNet ends in 2019, so the recent decade rests on Argo and on the Croatian monitoring CTD. On the matched annual series (27 years with at least 20 casts each), the Pettitt test places a level shift after 2014 ($p = 0.029$; Sect. 2.5). Occurrence averages 4.4 % of casts per year before the break and 17.1 % after, a factor of 3.9. The break year does not depend on how the matched set is assembled: restricting it to SeaDataNet and Argo alone, or adding the two Adriatic regional datasets, moves the means only between 4.4 and 4.8 % before and 17.1 and 17.2 % after, and leaves the break after 2014 and significant in every case.

The change is seasonal (Fig. 3B). Between 1950–1999 and 2000–2025, summer occurrence rises from 1.1 % (2 of 176 matched casts) to 30.8 % (297 of 965), and autumn from 4.0 % to 12.5 %, whereas winter occurrence stays at or below 1.3 % in both periods, indicating that winter mixing did not weaken comparably.

The properties of the detected cores changed alongside their frequency (Fig. 3C–F): the median core sits shallower than it did (19 m against 33 m), above a much stronger temperature inversion (median -0.64 against $-0.17\,^{\circ}\mathrm{C\,m}^{-1}$) and density step, while the salinity gradient that defines the feature is unchanged, so the modern events are shallower and more sharply capped rather than merely more frequent.

Two qualifications follow. The increase is roughly fourfold rather than the order of magnitude the raw series implies, because resolution matching raises the pre-2014 occurrence rate, against which the increase is measured, from about 1.5 % to about 4.4 %. The shift also cannot be pinned to 2017: it falls after 2014, so the defensible statement is that occurrence stepped up during the 2010s, with 2017 the most extreme year within an already elevated regime.

Resolution alone, however, does not explain the historical rarity. The 1188 casts from the 1990s that do meet the resolution criteria yield only 2.0 % detections, against 17.6 % in 2016–2025 on a comparable sample. The degradation experiment establishes only that the coarser part of the historical archive could not have detected these features at all, so absence from that part of the record is not evidence of absence from the ocean; the resolution-matched series remains the one that can size the increase, and it shows a threefold to fourfold rise.

3.6 Steric decomposition: the net contribution is negative

Thermosteric and halosteric height are decomposed separately from the Argo record, over 2014–2024, the most recent full decade with continuous float coverage. Over 0–1000 m (Table 3) the thermosteric trend is $+9.80 \pm 2.71$, the halosteric -15.21 ± 2.33 and the net $-5.41 \pm 2.49\,\mathrm{mm\,yr^{-1}}$ (Fig. A2): halosteric contraction dominates, and the steric term acts to lower local sea level rather than to raise it. On windows reaching back into the sparsely sampled early Argo years (2010 or 2012 to 2025) the net is also negative in the central estimate, at -1.4 to $-2.6\,\mathrm{mm\,yr^{-1}}$, but no longer distinguishable from zero. What holds on every window tested is the structure of the decomposition – thermosteric expansion significantly positive, halosteric contraction significantly negative and larger in magnitude – while the significantly negative net is a property of the well-sampled 2014–2024 decade.

Integration depth explains most of the apparent disagreement with published Mediterranean values. Recomputed on the 0–400 m layer used by Mohamed and Skliris (2022), the thermosteric rate is $+2.26 \pm 1.37\,\mathrm{mm\,yr^{-1}}$ against their eastern Mediterranean mean of $+2.13 \pm 0.41$: the rates agree once the layers match, and three quarters of the southern Adriatic thermosteric signal lies below 400 m. The halosteric term does not converge (-6.81 ± 2.55 against -0.75 ± 0.19), and that difference is real rather than methodological – Adriatic salinification over 2014–2024 far exceeds the eastern Mediterranean mean over 1993–2019. In the 600–1000 m layer the thermosteric and halosteric trends are individually well determined, $+5.7 \pm 0.9$ and $-5.6 \pm 1.0\,\mathrm{mm\,yr^{-1}}$, and compensate almost exactly, leaving a net of $+0.1 \pm 0.5\,\mathrm{mm\,yr^{-1}}$ that is consistent with zero. The compensation, not the residual, is the result, and it independently confirms the deep density result of Sect. 3.1.

These are decadal rates from a single platform over a window that spans the post-2017 episode, and they are not secular climate trends. To place them against a longer baseline, the same quantities are differenced between the two multiplatform climatologies of Sect. 2.2, 1950–1999 and 2000–2025. Converting that difference to a rate requires the time actually separating the two sets of casts. Their nominal midpoints are fifty years apart, but the casts are not evenly spread within either period: the 20th-century ones cluster in the 1990s, so the mean year of the casts entering each climatology is 1993 and 2013 and the effective separation is 19.8 years, not 50. On that baseline the thermosteric difference is $+7.6$ and the halosteric $-6.8\,\mathrm{mm\,yr^{-1}}$, with a net of $+0.8\,\mathrm{mm\,yr^{-1}}$ that is not distinguishable from zero and that changes sign with platform selection. Set against it, the recent decade differs from it in the halosteric term alone: the $-15.2\,\mathrm{mm\,yr^{-1}}$ of 2014–2024 is about 2.2 times the $-6.8\,\mathrm{mm\,yr^{-1}}$ of the long baseline, and between 2.0 and 2.6 times it whichever season of the climatology the comparison is made against. The thermosteric terms differ far less, $+9.8$ against $+7.6\,\mathrm{mm\,yr^{-1}}$, a ratio of 1.3. Nearly all of what distinguishes the recent decade is therefore in the salt.

3.7 Salt fingering: the change is below the LIW core

Sorted by depth, the double-diffusive diagnostics separate cleanly at the base of the classical LIW core (Table 5, Fig. 6).

Within the core itself, over 200–400 m, nothing changes that we can distinguish from sampling variability: the finger-favourable fraction is 55.3 % before 2017 and 60.1 % after ($p = 0.07$), and the vigorous fraction – levels with $R_\rho < 2$, at which

fingers transport appreciably – is 34.6 % against 33.1 % ($p = 0.37$), if anything slightly lower. Only stratification weakens, median N^2 falling by 26 %.

Below the core the picture changes. Over 400–600 m the finger-favourable fraction rises from 56.6 % to 63.0 % ($p = 0.001$) and the vigorous fraction from 28.0 % to 41.2 % ($p = 2 \times 10^{-11}$), while median N^2 falls by 60 %, from 2.50×10^{-6} to 0.99×10^{-6} s^{-2}. In the deep layer, 600–1000 m, the regime was already close to saturation in extent before 2017, occupying 92.1 % of levels, and does not expand further (88.7 % after); what changes there is vigour, and it changes more than anywhere else, from 10.7 % to 38.7 % ($p = 2 \times 10^{-77}$). The deep layer was thus always finger-favourable but only became finger-effective after 2017: the conditions allowed fingering throughout, and only recently has a large part of the layer reached the density ratios at which fingers actually transport salt.

This depth structure matches the one in Sect. 3.4. The deeper salinity maximum descended from a median 201 to 325 m, that is from the middle of the classical core toward its base, and the share of deeper maxima lying below 400 m rose from 16.1 % to 41.9 % over the same period. The layers in which fingering intensified are the layers the salt has moved into, and the core it has moved out of is the layer in which nothing changed.

Stratification is what drives this rather than any change in the temperature–salinity contrast: N^2 falls significantly in all three layers, and most sharply in the 400–600 m layer where the vigour increase is largest.

The intensification is progressive rather than a step at 2017. In the deep layer the median vigorous fraction per profile is 17 % in 2017 itself, close to the earlier level, rises through 2019 (24 %) to a maximum in 2021–2023 (51–61 %) and relaxes to about 30 % in 2025; the 400–600 m layer follows the same course about three years earlier, peaking in 2020. It therefore reaches the layer below the core before it reaches the deep layer, which is the order a downward transfer of salt requires.

4 Discussion

4.1 A coupled advective and local mechanism

The results are consistent with remote and local mechanisms acting together, and with neither alone. Progressively warmer and saltier Eastern Mediterranean source water supplies an increasingly saline reservoir at the southern boundary (Skliris et al., 2025; Schroeder et al., 2017), while local preconditioning determines how and where that salt is redistributed within the basin: reduced river discharge lowers the Adriatic freshwater budget (Verri et al., 2024), and the exceptional salinities of 2017 and their basin-scale preconditioning are documented by Mihanović et al. (2021). We have no observational budget for evaporation or winter mixing. The seasonal breakdown of Sect. 3.5 places the preconditioning in the warm season, since summer and autumn surface-lake occurrence rose sharply while winter occurrence did not, so the change acts on the summer surface layer rather than on winter convection.

The salinity-maximum result constrains the mechanism further. The deeper maximum stayed near its isopycnal, which is what advection of a denser saline core into a warming basin would produce, while the shallower one became much lighter as it salinified, which requires a different and shallower source. These are two pathways rather than one migrating feature, and a single-core description cannot represent both. Mihanović et al. (2021) see the same split in the 2015–2017 episode, with

new high-salinity water arriving nearer the surface from 2015 while the saline core deepened, though their excursion is far larger because they track individual floats through a particular sequence of years where we take a climatological median over multi-decadal periods.

Reported LIW depths vary too much between regions to serve as a baseline for any of this. The intermediate salinity maximum lies at 200–500 m for the Mediterranean as a whole and at 300–800 m in the western basin (Schroeder and Chiggiato, 2022), while Argo places it at 200–600 m Mediterranean-wide (Kubin et al., 2019) and at about 100–250 m in the eastern Mediterranean over 2015–2017 (Fach et al., 2021). The 200–400 m of the classical southern Adriatic description (Artegiani et al., 1997), the range we test against and the one our layers follow, sits within that spread.

One hypothesis follows, which the present data are consistent with but do not establish: that the depth-dependence of the amplification (Sect. 3.3) is the signature of this same split, with thermal amplification confined to the deep layers because renewal there is episodic while the upper layers are ventilated fast enough by air–sea exchange to track rather than exceed the Mediterranean mean, and haline amplification present through the column because salt arrives both at the surface and at depth. That the same sector emerges as the locus of Mediterranean-wide acceleration (Terzić and Vilibić, 2026c) is consistent with this reading, as is the depth structure of the double-diffusive result.

4.2 Density, sea level and ventilation

The steric decomposition bears directly on the sea level argument. With a net steric contribution of $-5.4 \pm 2.5\,\mathrm{mm\,yr^{-1}}$ the steric term opposes rather than drives local sea level rise, so any observed rise in the Southern Adriatic must be mass-driven. This is consistent with Verri et al. (2024), who attribute the recent northern Adriatic sea level decline to a regional water deficit, and with the near-exact deep thermal–haline compensation in Fig. 1. It rests on a single Argo decade: the sign is robust over 2014–2024, but whether it persists cannot be settled from this record.

Deep ventilation of the pit is episodic. From moorings over 2012–2022, Le Meur et al. (2025) identify gravity currents reaching the deep Southern Adriatic in only four years, 2012, 2017, 2018 and 2022; the first followed an exceptionally strong and prolonged bora outbreak that formed very cold, dense water (Mihanović et al., 2013). Deep properties therefore respond as a series of steps rather than as a gradual drift, each event resetting them before they relax again (Fig. 5), and the sign of the reset has changed: in the earlier regime (Querin et al., 2016) cascading water arrived cold and cooled the deep layer, whereas since 2017 it arrives only weakly cooled but much saltier and leaves the layer warmer and saltier than it found it (Terzić et al., 2025a). The deep trends of Sect. 3.6 are individually significant, but this saw-tooth is why a decade cannot show whether they are secular. Whether the shift toward haline-driven formation sustains ventilation, because saline water needs less cooling to sink, or degrades it, because the water so formed is warmer and carries less oxygen (Ingrosso et al., 2017; Chiarini et al., 2022), is not resolved by our data.

The double-diffusive result locates another mechanism, active in the recent decade. Finger-favourable water grows below the classical LIW core and not within it, which is where the deeper salinity maximum has moved (Sect. 3.7), because the density gradient there has weakened enough to let fingers reach full amplitude before ambient shear disrupts them. Salt fingering has therefore become more effective in the layer where the salt now arrives, and below it the deep layer, already saturated in extent,

tripled the fraction in which fingers actually transport salt. Salt descending out of the core meets a column newly capable of carrying it further down, though we have not measured a flux.

Amorim et al. (2024) report the same transition from the EMSO-E2M3A mooring in this pit, finger-favourable conditions rising from 27 % to 72 % of observations across the winter of 2016/17. Their 350–550 m layer straddles the base of the core, where we also find the change; recomputed on it our diagnostics rise from 48.6 to 60.2 % in extent and 29.1 to 38.8 % in vigour (Table 5). Both analyses find a significant increase there, which is as far as the agreement can be taken, since a mooring sampling one position continuously and a float array sampling the pit every few days do not measure the same quantity.

4.3 Biogeochemical and ecological implications

The following are plausible pathways, not effects quantified here, and we limit them to the changes reported above.

A near-surface salinity maximum has two competing effects on vertical exchange and our analysis resolves neither. It increases the density stability of the upper column, which acts to suppress exchange of oxygen, nutrients and carbon with the intermediate layers (Jacox and Edwards, 2011; Breitburg et al., 2018; Bourgeois et al., 2022), with consequences for production, microbial food webs and air–sea carbon exchange (Cantoni et al., 2024; Martellucci et al., 2025b); the record salinities of 2017 coincided with bacterial abundances several standard deviations from the mean (Beg Paklar et al., 2020), elevated salinity imposing osmotic stress that constrains growth directly. But salinity decreasing with depth beneath the maximum is itself finger-favourable, so the same feature may instead promote downward transport. Our diagnostics begin at 200 m and cannot say which dominates in the surface layer; dedicated observations there are required.

Whether the redistribution of the intermediate maxima promotes or suppresses production likewise depends on the upstream history of the inflowing water, on whether its nutrients were drawn down in the euphotic zone before it entered the basin (Ozer et al., 2022; Reich et al., 2026), which our results do not resolve.

For ecosystems, documented impacts and projected vulnerabilities should be kept apart. Three effects have been observed in the Adriatic: mass mortality linked to warming (Kružić et al., 2016), mussel mortality in coastal waters (Capriotti et al., 2025), and redistribution of benthic species toward northern coastlines (Matić-Skoko et al., 2022; Bellin and Rossi, 2024). Others remain projections: that further redistribution will be constrained by the basin's semi-enclosed geometry and by the limited cold-water refugia of the middle Adriatic depressions (Chiarini et al., 2022; Carlot et al., 2025), with consequences for the fisheries that exploit them (Martinelli et al., 2023; Kamberi et al., 2025). The link to aquaculture runs through the bottom-water warming and salinification documented in Sect. 3.1 rather than through climate change in general (Cetinić, 2024; Haberle et al., 2024).

4.4 Limitations

The climatological comparison rests on a changing observing system, and we have controlled for this where it is testable – by resolution matching for SSL detection, by degradation experiments for the salinity maxima, and by cruise-day clustering for the difference profiles – but not everywhere. Northern Adriatic salinity remains the weakest element, because 20th-century sampling is concentrated on the western side of a basin with a strong east–west salinity gradient. The Argo-based steric and

double-diffusive results describe the Southern Adriatic Pit over a single decade, and a decade cannot separate a secular climate trend from the episodic cycle of deep renewal.

The larger gap is that this is an ocean-side analysis throughout: we establish when the changes occurred and how they are distributed in the vertical, but not what forced them. Wintertime turbulent heat flux anomalies over the northern Adriatic formation region do not share a common cooling signature across the recent cascading years – 2018 and 2022 carry positive anomalies relative to the 1980–2010 baseline, so the density required for cascading in those years cannot have come from heat loss alone (Terzić et al., 2025a). That is consistent with the mechanism proposed above but is not an attribution of it, and the flux estimate is coarse: reanalyses at this resolution underestimate the cooling along the bora jets (Denamiel et al., 2021), where much of the relevant heat loss occurs. Establishing how much of the change reported here follows from bora frequency, evaporation and river discharge requires a dedicated surface-flux and freshwater budget over the formation regions, resolved finely enough to capture the jets. Until that is done, the mechanism of Sect. 4.1 remains a hypothesis rather than an attribution.

5 Conclusions

Three findings are supported by the analyses presented here. First, southern Adriatic warming and salinification between 1950–1999 and 2000–2025 are significant at every depth and season, but the amplification relative to the Mediterranean – the ratio of the median within-window trend in the southern Adriatic to the median across the other Mediterranean sub-basins, computed with one pipeline (Sect. 3.3) – is depth-dependent: 6.1-fold for temperature at 700–1200 m and about half the basin median above 200 m, while haline amplification is present through the whole column, reaching 4.3-fold at the surface and 3.8-fold at 700–1200 m. Second, the increase in near-surface salinity maxima is a genuine level shift after 2014, roughly fourfold, and is demonstrable only once vertical resolution is controlled for. The coarser part of the historical archive could not have detected these features at all, yet even among the historical casts that could, occurrence was far rarer: 2.0 % in the 1990s against 17.6 % in 2016–2025, comparing only casts of comparable vertical resolution. Third, the intermediate salinity maximum has lost the dominant band of the classical description: the share of detected maxima within 100–200 m falls from 42 % to 16 % between the periods, while the share of casts carrying two maxima shows no consistent change. Where two coexist they move apart, the deeper one descending from a median 201 to 325 m while remaining close to its isopycnal and the shallower one rising from 100 to 78 m; only the shallower one becomes markedly lighter as it salinifies, which points to a different and shallower source.

Two further results bear on the mechanism. The steric contribution in the Southern Adriatic Pit over 2014–2024 is $-5.4 \pm 2.5\,\mathrm{mm\,yr^{-1}}$, negative rather than positive, so local sea level rise must be mass-driven. Moreover, salt fingering has intensified below the classical intermediate core and not within it, in vigour more than in extent, driven by a weakening of stratification measurable in N^2; the layers into which the deeper salinity maximum has descended are therefore also those newly capable of carrying salt further down.

The consequences for ventilation, biogeochemistry, regional climate feedbacks and ecosystems remain hypotheses. Testing them requires sustained in situ observing at a vertical resolution able to resolve the features described here, and high-resolution coupled physical–biogeochemical modelling able to represent episodic deep renewal. It would also be served by an update of

the SeaDataNet Mediterranean aggregation, which currently ends in 2019: the most recent six years of shipborne hydrography are precisely those in which the changes reported here developed, and at present only Argo covers them.

Code and data availability. The cleaned in situ data are archived by Terzić and Vilibić (2026a) and the analysis code and derived tables by Terzić and Vilibić (2026b). The in situ record ends in 2019; the 2020–2025 part of the 2000–2025 window is supplied by Argo. SeaDataNet Mediterranean aggregated dataset SDC_MED_DATA_TS_V2 is available from https://www.seadatanet.org; Argo data from Euro-Argo ERIC, https://www.euro-argo.eu. Argo floats used are listed in Table 4. Floats 6903805 and 6901865 were excluded from the steric analysis because their profiles do not reach 1000 dbar in the Southern Adriatic Pit; all other ascending profiles reaching 1000 dbar were retained.

Author contributions. ET: conceptualisation, methodology, formal analysis, investigation, data curation, software, visualisation, writing – original draft, writing – review and editing. IV: conceptualisation, methodology, writing – original draft, writing – review and editing, funding acquisition.

Competing interests. The authors declare that they have no competing interests.

Acknowledgements. We are grateful to all researchers who developed the concepts and collected the observations on which this study rests. We acknowledge the provision of temperature and salinity data by the SeaDataNet Pan-European Infrastructure, Euro-Argo ERIC, the Institute of Oceanography and Fisheries, the Ruđer Bošković Institute, and Italian marine research institutions. Comments raised by two anonymous reviewers greatly improved the quality of the article. This research was supported by the Croatian Science Foundation through projects GLOMETS (IP-2022-10-3064) and C3PO (IP-2022-10-9139) and the incoming mobility scheme for postdoctoral researchers (MOBDOL-2023-12), the Interreg Italy–Croatia Programme 2021–2027 project AdriaClimPlus (ITHR0200333), and the EU NextGeneration project AdriaClimRisk (PK.3.4.17.0001).

References

Amorim, F. L. L., Le Meur, J., Wirth, A., and Cardin, V.: Tipping of the double-diffusive regime in the southern Adriatic Pit in 2017 in connection with record high-salinity values, Ocean Sci., 20, 463-474, https://doi.org/10.5194/os-20-463-2024, 2024.

Artegiani, A., Bregant, D., Paschini, E., Pinardi, N., Raicich, F., Russo, A.: The Adriatic Sea general circulation. Part I: Air–sea interactions and water mass structure. J. Phys. Oceanogr., 27, 1492–1514, https://doi.org/10.1175/1520-0485(1997)027<1492:TASGCP>2.0.CO;2, 1997.

Beg Paklar, G., Vilibić, I., Grbec, B., Matić, F., Mihanović, H., Džoić, T., et al.: Record-breaking salinities in the middle Adriatic during summer 2017 and concurrent changes in the microbial food web. Prog. Oceanogr., 185, 102345, https://doi.org/10.1016/j.pocean.2020.102345, 2020.

Bellin, N., Rossi, V.: Modeling the effects of climate change on the habitat suitability of Mediterranean gorgonians. Biodivers. Conserv., 33, 929–948, https://doi.org/10.1007/s10531-024-02779-z, 2024.

Bourgeois, T., Goris, N., Schwinger, J., Tjiputra, J. F.: Stratification constrains future heat and carbon uptake in the Southern Ocean between 30°S and 55°S. Nat. Commun., 13, 340, https://doi.org/10.1038/s41467-022-27979-5, 2022.

Breitburg, D., Levin, L. A., Oschlies, A., Grégoire, M., Chavez, F. P., Conley, D. J.: Declining oxygen in the global ocean and coastal waters. Science, 359, 6371, https://doi.org/10.1126/science.aam7240, 2018.

Bretherton, C. S., Widmann, M., Dymnikov, V. P., Wallace, J. M., and Bladé, I.: The effective number of spatial degrees of freedom of a time-varying field, J. Climate, 12, 1990-2009, https://doi.org/10.1175/1520-0442(1999)012<1990:TENOSD>2.0.CO;2, 1999.

Cantoni, C., De Vittor, C., Faganeli, J., Giani, M., Kovač, N., Malej, A.: Carbonate system and acidification of the Adriatic Sea. Mar. Chem., 267, 104462, https://doi.org/10.1016/j.marchem.2024.104462, 2024.

Capriotti, M., Bracchetti, L., Cocci, P., Mazzocchi, V., Fazzini, M., Corvaro, F., et al.: In situ investigation of ecological and molecular stress mechanisms triggered by marine heat waves in Adriatic populations of the Mediterranean mussel. Diversity, 17, 385, https://doi.org/10.3390/d17060385, 2025.

Carlot, J., Galobart, C., Gómez-Gras, D., Santamaría, J., Golo, R., Siniet, M., et al.: Vulnerability of benthic trait diversity across the Mediterranean Sea following mass mortality events. Nat. Commun., 16, 1571, https://doi.org/10.1038/s41467-025-55949-0, 2025.

Cetinić, A. B.: Shellfisheries in Croatia: from manual collection to contemporary practices, Naše More, 71, 154-165, https://doi.org/10.17818/NM/2024/3.8, 2024.

Chiarini, M., Guicciardi, S., Zacchetti, L., Domenichetti, F., Canduci, G., Angelini, S., et al.: Short-term evaluation of changes in fisheries management measures in the Pomo/Jabuka Pits area. Sustainability, 14, 7742, https://doi.org/10.3390/su14137742, 2022.

Civitarese, G., Gačić, M., Lipizer, M., Borzelli, G. L. E.: On the impact of the BiOS on the Adriatic and Ionian Seas. Biogeosciences, 7, 3987–3997, https://doi.org/10.5194/bg-7-3987-2010, 2010.

Civitarese, G., Gačić, M., Batistić, M., et al.: The BiOS mechanism: History, theory, implications. Prog. Oceanogr., 216, 103056, https://doi.org/10.1016/j.pocean.2023.103056, 2023.

Cushman-Roisin, B. and Korotenko, K. A.: Mesoscale-resolving simulations of summer and winter bora events in the Adriatic Sea, J. Geophys. Res.-Oceans, 112, C11S91, https://doi.org/10.1029/2006JC003516, 2007.

Denamiel, C., Tojčić, I., and Vilibić, I.: Balancing accuracy and efficiency of atmospheric models in the northern Adriatic during severe bora events, J. Geophys. Res.-Atmos., 126, e2020JD033516, https://doi.org/10.1029/2020JD033516, 2021.

Fach, B. A., Orek, H., Yilmaz, E., Tezcan, D., Salihoglu, I., Salihoglu, B., et al.: Water mass variability and Levantine Intermediate Water formation in the Eastern Mediterranean between 2015 and 2017, J. Geophys. Res.-Oceans, 126, e2020JC016472, https://doi.org/10.1029/2020JC016472, 2021.

Gačić, M., Civitarese, G., Miserocchi, S., Cardin, V., Crise, A., and Mauri, E.: The open-ocean convection in the Southern Adriatic: a controlling mechanism of the spring phytoplankton bloom, Cont. Shelf Res., 22, 1897–1908, https://doi.org/10.1016/S0278-4343(02)00050-X, 2002.

Gačić, M., Borzelli, G. L. E., Civitarese, G., Cardin, V., and Yari, S.: Can internal processes sustain reversals of the ocean upper circulation? The Ionian Sea example, Geophys. Res. Lett., 37, L09608, https://doi.org/10.1029/2010GL043216, 2010.

Haberle, I., Hackenberger, D. K., Djerdj, T., Bavčević, L., Geček, S., Hackenberger, B. K., et al.: Effects of climate change on gilthead seabream aquaculture in the Mediterranean, Aquaculture, 578, 740052, https://doi.org/10.1016/j.aquaculture.2023.740052, 2024.

Holt, J., Katavouta, A., Hopkins, J., Amoudry, L. O., Appendini, C. M., Arneborg, L., et al.: Future climate projections in the global coastal ocean, Prog. Oceanogr., 235, 103497, https://doi.org/10.1016/j.pocean.2025.103497, 2025.

Ingrosso, G., Bensi, M., Cardin, V., and Giani, M.: Anthropogenic CO2 in a dense water formation area of the Mediterranean Sea, Deep-Sea Res. Part I, 123, 118–128, https://doi.org/10.1016/j.dsr.2017.04.004, 2017.

IOC, SCOR and IAPSO: The international thermodynamic equation of seawater – 2010: Calculation and use of thermodynamic properties, IOC Manuals and Guides No. 56, UNESCO, Paris, https://doi.org/10.25607/OBP-1662, 2010.

Jacox, M. G. and Edwards, C. A.: Effects of stratification and shelf slope on nutrient supply in coastal upwelling regions, J. Geophys. Res.-Oceans, 116, C03019, https://doi.org/10.1029/2010JC006547, 2011.

Juza, M., Fernández-Mora, À., Tintoré, J.: Sub-regional marine heat waves in the Mediterranean Sea from observations: long-term surface changes, sub-surface and coastal responses, Front. Mar. Sci., 9, 785771, https://doi.org/10.3389/fmars.2022.785771, 2022.

Kamberi, E., Hala, E., and Möllmann, C.: Evidence of climate-driven regime shifts in Adriatic Sea fisheries, Sci. Mar., 89, e108, https://doi.org/10.3989/scimar.05566.108, 2025.

Kružić, P., Rodić, P., Popijač, A., and Sertić, M.: Impacts of temperature anomalies on mortality of benthic organisms in the Adriatic Sea, Mar. Ecol., 37, 1190–1209, https://doi.org/10.1111/maec.12293, 2016.

Kubin, E., Poulain, P.-M., Mauri, E., Menna, M., and Notarstefano, G.: Levantine intermediate and Levantine deep water formation: an Argo float study from 2001 to 2017, Water, 11, 1781, https://doi.org/10.3390/w11091781, 2019.

Kunze, E.: Limits on growing, finite-length salt fingers: a Richardson number constraint, J. Mar. Res., 45, 533–556, https://doi.org/10.1357/002224087788326885, 1987.

Le Meur, J., Wirth, A., de Mendoza, F. P., Miserocchi, S., and Cardin, V.: Intermittent supply of dense water to the deep South Adriatic Pit: an observational study, Front. Mar. Sci., 12, 1516780, https://doi.org/10.3389/fmars.2025.1516780, 2025.

Manca, B. B., Burca, M., Giorgetti, A., Coatanoan, C., Garcia, M. J., and Iona, A.: Physical and biochemical averaged vertical profiles in the Mediterranean regions: an important tool to trace the climatology of water masses and to validate incoming data from operational oceanography, J. Mar. Syst., 48, 83–116, https://doi.org/10.1016/j.jmarsys.2003.11.025, 2004.

Marini, M., Russo, A., Paschini, E., Grilli, F., and Campanelli, A.: Short-term physical and chemical variations in the bottom water of middle Adriatic depressions, Clim. Res., 31, 227–237, https://doi.org/10.3354/cr031227, 2006.

Martellucci, R., Dentico, C., Coppola, L., Skjelvan, I., Giani, M., Pensieri, S., et al.: Air–sea CO2 exchange in the Eastern Atlantic and the Mediterranean Sea based on autonomous surface measurements, Front. Mar. Sci., 12, 1633617, https://doi.org/10.3389/fmars.2025.1633617, 2025b.

Martinelli, M., Zacchetti, L., Belardinelli, A., Domenichetti, F., Scarpini, P., Penna, P., et al.: Changes in abundance and distribution of the sea pen, Funiculina quadrangularis, in the central Adriatic Sea (Mediterranean basin) in response to variations in trawling intensity, Fishes, 8, 347, https://doi.org/10.3390/fishes8070347, 2023.

Matić-Skoko, S., Pavičić, M., Šepić, J., Janeković, I., Vrdoljak, D., Vilibić, I., et al.: Impacts of sea bottom temperature on CPUE of European lobster Homarus gammarus (Linnaeus, 1758; Decapoda, Nephropidae) in the Eastern Adriatic Sea, Front. Mar. Sci., 9, 891197, https://doi.org/10.3389/fmars.2022.891197, 2022.

Maze, G. and Balem, K.: argopy: A Python library for Argo ocean data analysis, J. Open Source Softw., 5, 2425, https://doi.org/10.21105/joss.02425, 2020.

Mihanović, H., Vilibić, I., Carniel, S., Tudor, M., Russo, A., Bergamasco, A., et al.: Exceptional dense water formation on the Adriatic shelf in the winter of 2012, Ocean Sci., 9, 561–572, https://doi.org/10.5194/os-9-561-2013, 2013.

Mihanović, H., Vilibić, I., Šepić, J., Matić, F., Ljubešić, Z., Mauri, E., et al.: Observation, preconditioning and recurrence of exceptionally high salinities in the Adriatic Sea, Front. Mar. Sci., 8, 672210, https://doi.org/10.3389/fmars.2021.672210, 2021.

Mohamed, B. and Skliris, N.: Steric and atmospheric contributions to interannual sea level variability in the eastern Mediterranean Sea over 1993-2019, Oceanologia, 64, 50-62, https://doi.org/10.1016/j.oceano.2021.09.001, 2022.

Ozer, T., Rahav, E., Gertman, I., Sisma-Ventura, G., Silverman, J., and Herut, B.: Relationship between thermohaline and biochemical patterns in the Levantine upper and intermediate water masses, Southeastern Mediterranean Sea (2013–2021), Front. Mar. Sci., 9, 958924, https://doi.org/10.3389/fmars.2022.958924, 2022.

Pettitt, A. N.: A non-parametric approach to the change-point problem, J. Roy. Stat. Soc. C-App., 28, 126-135, https://doi.org/10.2307/2346729, 1979.

Pranić, P., Denamiel, C., Janeković, I., and Vilibić, I.: Multi-model analysis of the Adriatic dense-water dynamics, Ocean Sci., 19, 649–670, https://doi.org/10.5194/os-19-649-2023, 2023.

Querin, S., Bensi, M., Cardin, V., Solidoro, C., Bacer, S., Mariotti, L., et al.: Saw-tooth modulation of the deep-water thermohaline properties in the southern Adriatic Sea, J. Geophys. Res.-Oceans, 121, 4585–4600, https://doi.org/10.1002/2015JC011522, 2016.

Reich, T., Belkin, N., Sisma-Ventura, G., Hauzer, H., Berman-Frank, I., and Rahav, E.: Does oligotrophy favor chemoautotrophy over photoautotrophy?, Prog. Oceanogr., 241, 103633, https://doi.org/10.1016/j.pocean.2025.103633, 2026.

Richardson, C. M., Peucker-Ehrenbrink, B., Wyatt, S., Bourbonnais, A., Hatje, V., Frey, C., et al.: Effects of climate change on river and groundwater nutrient inputs to the coastal ocean, Commun. Earth Environ., 6, 761, https://doi.org/10.1038/s43247-025-02594-6, 2025.

Roether, W., Manca, B. B., Klein, B., Bregant, D., Georgopoulos, D., Beitzel, V., et al.: Recent changes in eastern Mediterranean deep waters, Science, 271, 333–335, https://doi.org/10.1126/science.271.5247.333, 1996.

Schlitzer, R., Roether, W., Oster, H., Junghaus, H.-G., Hausmann, M., Johannsen, H., et al.: Chlorofluoromethane and oxygen in the Eastern Mediterranean, Deep-Sea Res., 38, 1531–1551, https://doi.org/10.1016/0198-0149(91)90088-W, 1991.

Schmitt, R. W.: Double diffusion in oceanography, Annu. Rev. Fluid Mech., 26, 255-285, https://doi.org/10.1146/annurev.fl.26.010194.001351, 1994.

Schroeder, K. and Chiggiato, J. (Eds.): Oceanography of the Mediterranean Sea: An Introductory Guide, Elsevier, Amsterdam, 558 pp., https://doi.org/10.1016/C2020-0-01415-3, 2022.

Schroeder, K., Chiggiato, J., Josey, S. A., Borghini, M., Aracri, S., and Sparnocchia, S.: Rapid response to climate change in a marginal sea, Sci. Rep., 7, 4065, https://doi.org/10.1038/s41598-017-04455-5, 2017.

SeaDataNet: Data quality control procedures, version 2.0, https://www.seadatanet.org/content/download/596/file/SeaDataNet_QC_procedures_V2_(May_2010).pdf, 2010.

Simoncelli, S., Schaap, D., and Schlitzer, R.: Mediterranean Sea – Temperature and salinity Historical Data Collection SeaDataCloud V2 (SDC_MED_DATA_TS_V2) [Dataset], SeaDataNet, https://doi.org/10.12770/2a2aa0c5-4054-4a62-a18b-3835b304fe64, 2020.

Skliris, N., Marsh, R., Breedon, M., and Josey, S. A.: Accelerated warming and salinification of the Mediterranean Sea: Implications for dense water formation, J. Mar. Sci. Eng., 13, 25, https://doi.org/10.3390/jmse13010025, 2025.

Terzić, E., Cardin, V., Le Meur, J., Dunić, N., Vodopivec, M., and Vilibić, I.: Unprecedented warming and salinization observed in the deep Adriatic, Limnol. Oceanogr. Lett., 10, 888–898, https://doi.org/10.1002/lol2.70051, 2025a.

Terzić, E., Gardiol, C., and Vilibić, I.: Surface saline lakes in the Mediterranean Sea, Ocean Sci., 21, 1441–1459, https://doi.org/10.5194/os-21-1441-2025, 2025b.

Terzić, E. and Vilibić, I.: Cleaned Adriatic in situ hydrographic data (1952–2023) for a Mediterranean thermohaline acceleration analysis [Dataset], Zenodo, https://doi.org/10.5281/zenodo.20345373, 2026a.

Terzić, E. and Vilibić, I.: MedClim analysis code for Mediterranean thermohaline acceleration analysis [Software], Zenodo, https://doi.org/10.5281/zenodo.20410481, 2026b.

Terzić, E. and Vilibić, I.: Observational evidence for accelerated warming and salinification propagating into the deep Mediterranean, Geophys. Res. Lett., 53, e2026GL124518, https://doi.org/10.1029/2026GL124518, 2026c.

Tintoré, J., Pinardi, N., Álvarez-Fanjul, E., Aguiar, E., Álvarez-Berastegui, D., Bajo, M., et al.: Challenges for sustained observing and forecasting systems in the Mediterranean Sea, Front. Mar. Sci., 6, 568, https://doi.org/10.3389/fmars.2019.00568, 2019.

Verri, G., Furnari, L., Gunduz, M., Senatore, A., Santos da Costa, V., De Lorenzis, A., et al.: Climate projections of the Adriatic Sea: role of river release, Front. Climate, 6, 1368413, https://doi.org/10.3389/fclim.2024.1368413, 2024.

Vilibić, I., Matijević, S., Šepić, J. and Kušpilić, G.: Changes in the Adriatic oceanographic properties induced by the Eastern Mediterranean Transient, Biogeosci., 9, 2085–2097, https://doi.org/10.5194/bg-9-2085-2012, 2012.

Vilibić, I., Zemunik, P., Šepić, J., Dunić, N., Marzouk, O., Mihanović, H., et al.: Present-climate trends and variability in thermohaline properties of the northern Adriatic shelf, Ocean Sci., 15, 1351–1362, https://doi.org/10.5194/os-15-1351-2019, 2019.

Vilibić, I., Pranić, P. and Denamiel, C.: North Adriatic Dense Water: lessons learned since the pioneering work of Mira Zore-Armanda 60 years ago, Acta Adriat., 64, 53–78, https://doi.org/10.32582/aa.64.1.11, 2023.

Wagawa, T., Igeta, Y. and Abe, S.: Warming and springtime freshening trend in the southeastern Sea of Japan revealed by observational data, Geophys. Res. Lett., 52, e2025GL118631, https://doi.org/10.1029/2025GL118631, 2025.

Wang, G., Cheng, L., Boyer, T., and Li, C.: Halosteric sea level changes during the Argo era, Water, 9, 484, https://doi.org/10.3390/w9070484, 2017.

Wong, A., Keeley, R., and Carval, T., and the Argo Management Team: Argo Quality Control Manual for CTD and Trajectory Data. Version 3.7. https://doi.org/10.13155/33951, 2023.

Zore-Armanda, M.: Les masses d'eau de la mer Adriatique, Acta Adriat., 10, 5–88, 1963.

Table 1. Observational dataset inventory. Counts are retained casts entering the climatologies behind Figs. 1–2. DJ1 and DJ3 are the northern and southern Adriatic polygons defined in the `Basins` package and labelled after the sub-basin nomenclature of Manca et al. (2004); they follow the coastline and bathymetry rather than that paper's boundaries (Sect. 2.2). Bounding boxes are given because the regions are polygons rather than rectangles; their full extent is shown in Figs. 1 and 2. In (b), note the 20th-century summer count in DJ3 (444), the sparsest season–period combination. In (e), the shallowest bin centre of 5 m spans the layer in which the two periods are sampled least alike, and is not interpreted in summer (Sect. 3.1).

(a) Casts by source, region and period

Region	Source	1950–1999	2000–2025	Total
DJ1	SeaDataNet	8903	11014	19917
DJ1	RBI northern Adriatic transect 1979–2018	984	1037	2021
DJ1	IOR Adriatic database 1987–2019	731	829	1560
DJ1	Croatian MSFD / JADMON CTD 2019–2023	0	429	429
DJ1	Argo	0	293	293
DJ3	SeaDataNet	3291	3289	6580
DJ3	Argo	0	2946	2946
DJ3	IOR Adriatic database 1987–2019	141	323	464
DJ3	Croatian MSFD / JADMON CTD 2019–2023	0	96	96

(b) Casts by season

Region	Period	JFM	AMJ	JAS	OND	Total
DJ1	1950–1999	1946	2726	3847	2099	10618
DJ1	2000–2025	3388	2639	4104	3471	13602
DJ3	1950–1999	1028	1163	444	797	3432
DJ3	2000–2025	1227	1721	1852	1854	6654

(c) Casts by maximum depth reached [m]

Region	Period	0–50	50–200	200–600	600–1000	$\geq$1000
DJ1	1950–1999	9931	687	0	0	0
DJ1	2000–2025	12697	905	0	0	0
DJ3	1950–1999	151	1009	804	1076	392
DJ3	2000–2025	1171	900	1005	2618	960

(d) Region boundaries (polygon bounding box)

Region	Name	Longitude	Latitude
DJ1	Northern Adriatic	12.065–15.538 °E	43.623–45.809 °N
DJ3	Southern Adriatic	15.888–20.021 °E	39.790–42.940 °N

(e) Processing parameters

Bin centres (m): 5, 10, 20, 30, 40, 50, 75, 100, 125, 150, 200, 250, 300, 400, 500, 600, 700, 800, 900, 1000, 1100, 1200. Minimum fractional coverage per level: 0.05 (both T and S). Second-pass outlier rejection: 1.0 standard deviation. Accepted quality flags: 1 and 2 (SeaDataNet and Argo). Equation of state: TEOS-10; σ_0 referenced to 0 dbar.

Table 2. Warming and salinification rates for 2000–2025, Adriatic against Mediterranean, from an identical pipeline, binning, quality control and estimator on both sides. Mediterranean values are the median across sub-basins outside the Adriatic, with the interquartile range in brackets; Adriatic values are the median across depth bins within the layer. Trends resting on fewer than 24 months are excluded, which is why DJ1 has no entry below 200 m. DJ1 is reported only to 50 m, because below that the shelf rests on 905 casts against 12 697 above it (Sect. 2.3).

Variable	Layer	DJ1	DJ3	Mediterranean	DJ1/Med	DJ3/Med
T [°C decade^{-1}]	5–50 m	$+0.600$	$+0.223$	$+0.406$ ($+0.264$ to $+0.509$)	1.5	0.5
T	75–200 m	—	$+0.249$	$+0.342$ ($+0.266$ to $+0.400$)	—	0.7
T	250–600 m	—	$+0.333$	$+0.222$ ($+0.166$ to $+0.291$)	—	1.5
T	700–1200 m	—	$+0.429$	$+0.070$ ($+0.037$ to $+0.111$)	—	**6.1**
S [decade^{-1}]	5–50 m	$+0.154$	$+0.222$	$+0.051$ (-0.032 to $+0.097$)	3.0	**4.3**
S	75–200 m	—	$+0.101$	$+0.076$ ($+0.022$ to $+0.112$)	—	1.3
S	250–600 m	—	$+0.125$	$+0.067$ ($+0.055$ to $+0.083$)	—	1.9
S	700–1200 m	—	$+0.122$	$+0.032$ ($+0.014$ to $+0.044$)	—	**3.8**

Table 3. Steric sea level trends in the Southern Adriatic Pit, 2014–2024, from deseasoned monthly means of Argo profiles. Intervals are 95 % confidence intervals on the trend, computed with an effective sample size that accounts for residual autocorrelation (Sect. 2.8); they are not standard deviations of the underlying series, and are wide because the effective sample size is a fraction of the number of months. Eastern Mediterranean values are from Mohamed and Skliris (2022) for 1993–2019 and are shown on their own integration layer.

Layer / source	Thermosteric [mm yr^{-1}]	Halosteric [mm yr^{-1}]	Net [mm yr^{-1}]
This study, 0–1000 m	$\mathbf{+9.80 \pm 2.71}$	$\mathbf{-15.21 \pm 2.33}$	$\mathbf{-5.41 \pm 2.49}$
This study, 0–700 m	$+5.30 \pm 2.19$	-11.03 ± 2.54	-5.73 ± 2.28
This study, 0–400 m	$+2.26 \pm 1.37$	-6.81 ± 2.55	-4.55 ± 1.73
This study, 600–1000 m	$+5.7 \pm 0.9$	-5.6 ± 1.0	$+0.1 \pm 0.5$
Eastern Mediterranean, 0–400 m, 1993–2019	$+2.13 \pm 0.41$	-0.75 ± 0.19	—

Table 4. Argo floats contributing to the Southern Adriatic Pit analyses (steric decomposition and subsurface salinity maxima), restricted to ascending profiles reaching at least 1000 dbar.

WMO	Profiles	First	Last	Max. pressure [dbar]
1900848	13	2010-04	2014-04	1184.6
3901978	16	2018-10	2019-09	1220.9
3902626	34	2024-12	2025-09	1227.0
6900979	8	2013-08	2013-11	1173.0
6901040	25	2012-03	2014-05	1216.0
6901822	100	2013-03	2017-12	1227.9
6901827	68	2013-09	2018-05	1207.6
6901862	6	2015-03	2015-04	1018.4
6902848	46	2020-04	2022-11	1223.9
6903178	65	2015-10	2016-08	1222.7
6903197	27	2016-04	2017-02	1016.5
6903236	3	2018-11	2018-11	1213.3
6903250	57	2018-10	2021-01	1020.9
6903781	8	2020-07	2021-01	1228.0
6903799	166	2021-05	2025-09	1230.8
6903821	12	2024-07	2025-01	1151.3
6903825	40	2022-12	2025-08	1017.8

Table 5. Salt-finger diagnostics by layer in the Southern Adriatic Pit, from 694 Argo profiles split before and from 2017 (257 and 437 profiles). Layers are those used throughout the paper: the classical 200–400 m LIW salinity-maximum range (Sect. 3.4), the 400–600 m layer immediately below it, and the deep layer. Extent is the percentage of levels in the salt-finger regime, vigour the percentage with $R_\rho < 2$, and N^2 the median squared buoyancy frequency. Values are means across profiles and p-values are two-sided Mann–Whitney tests on the per-profile layer statistics; those below 0.05 are in bold. Nothing changes significantly inside the core. The last row is the 350–550 m layer instrumented at the EMSO-E2M3A mooring, given only so that our diagnostics can be compared with Amorim et al. (2024) in Sect. 4.2; it straddles the base of the core and is not one of our layers.

	Extent [%]			Vigour [%]			N^2 [10^{-6} s^{-2}]		
Layer	<2017	≥2017	p	<2017	≥2017	p	<2017	≥2017	p
200–400 m *(LIW core)*	55.3	60.1	0.068	34.6	33.1	0.37	1.96	1.44	$\mathbf{7 \times 10^{-9}}$
400–600 m	56.6	63.0	**0.001**	28.0	41.2	$\mathbf{2 \times 10^{-11}}$	2.50	0.99	$\mathbf{4 \times 10^{-43}}$
600–1000 m	92.1	88.7	$\mathbf{8 \times 10^{-24}}$	10.7	38.7	$\mathbf{2 \times 10^{-77}}$	2.55	1.72	$\mathbf{2 \times 10^{-88}}$
350–550 m (mooring layer)	*48.6*	*60.2*	8×10^{-10}	*29.1*	*38.8*	2×10^{-7}	*2.51*	*0.96*	2×10^{-39}

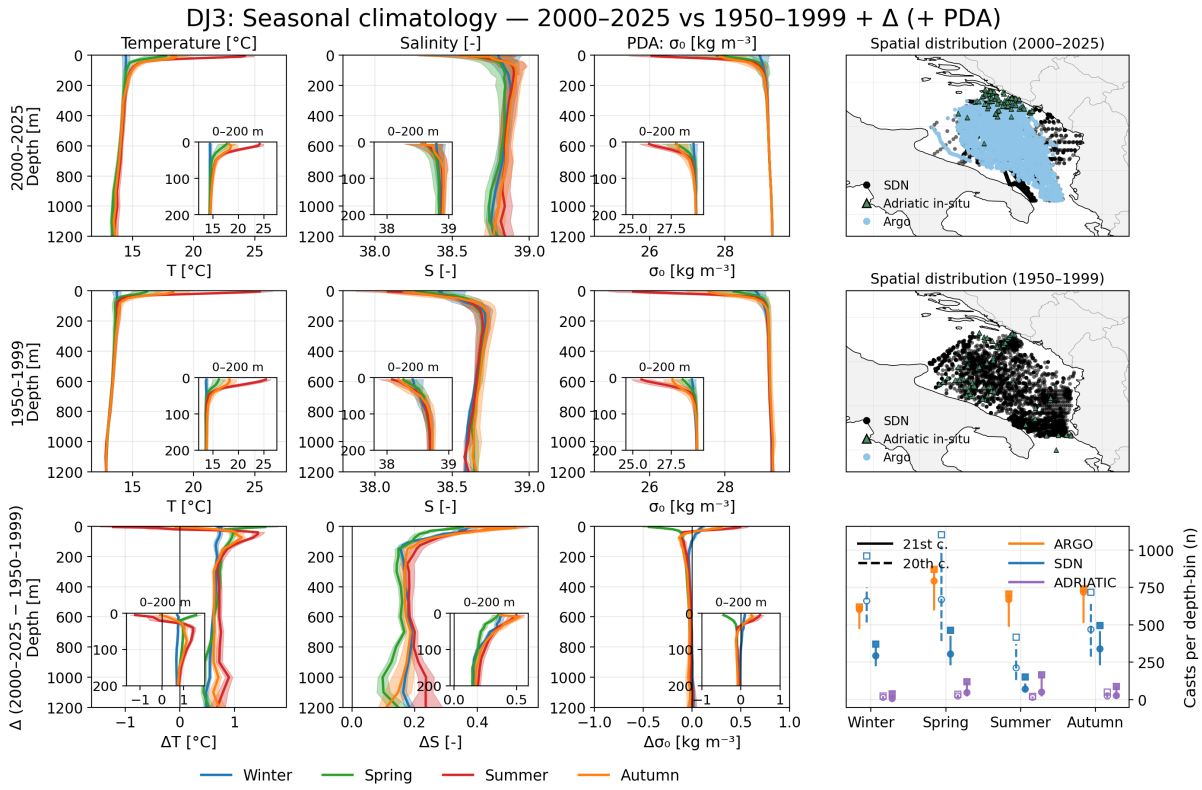


Figure 1. Seasonal climatology of the southern Adriatic (DJ3, Sect. 2.2) from all available in situ sources. Rows: 2000–2025 (top), 1950–1999 (middle), and their difference (bottom); columns: temperature, salinity, potential density anomaly, and observational support. Colours denote seasons. Insets expand the upper 200 m. In the two period rows the shading is ± 1 standard deviation, the spread of the observations contributing to each level. In the difference row it is the 95 % confidence interval on the difference, obtained from a bootstrap over cruise-days so that casts taken within one cruise are not counted as independent (Sect. 2.3); that is the band against which significance should be judged. The right column shows the spatial distribution of casts by source for each period, and the sampling-support panel gives casts per depth bin by platform and season: means as squares, medians as circles, ranges as vertical lines, solid for 2000–2025 and dashed for 1950–1999.

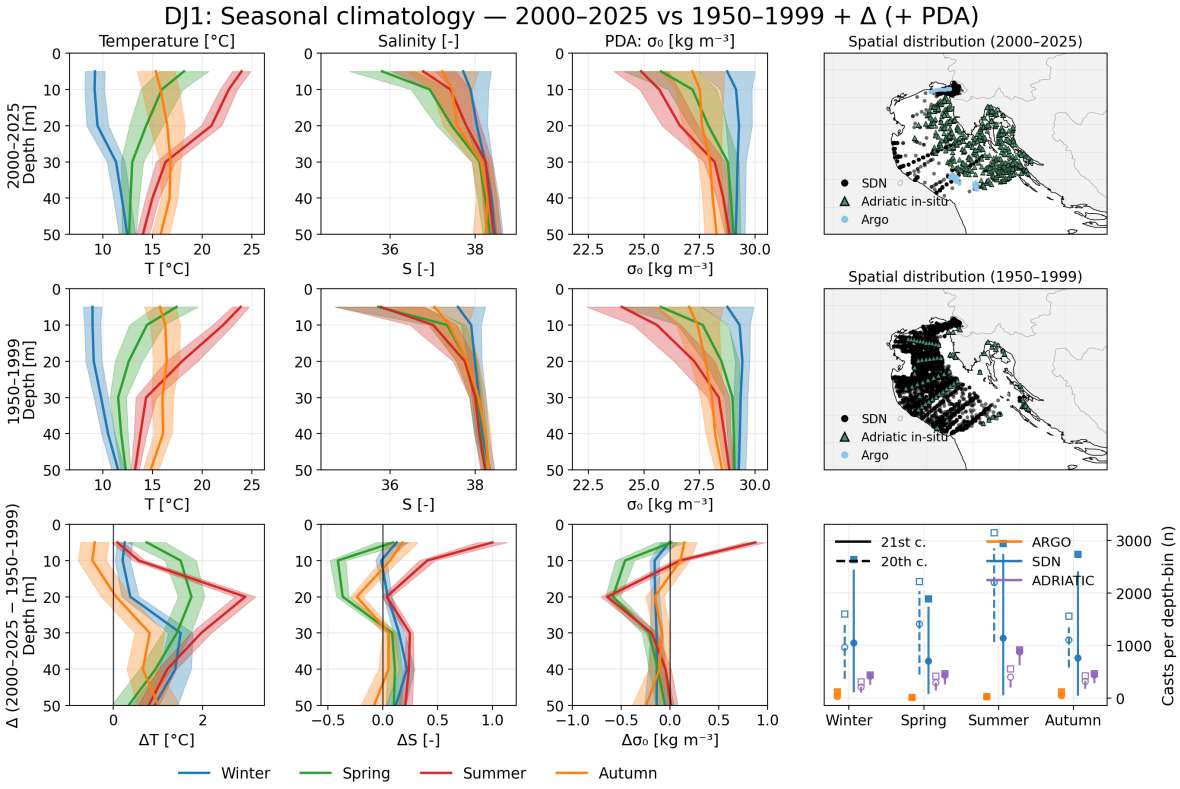


Figure 2. As Fig. 1, but for the northern Adriatic (DJ1, Sect. 2.2) and restricted to 0–50 m. Below 50 m the northern shelf carries fewer than 700 casts per period against more than 12 000 above it (Table 1), and the fitted trend changes sign with the analysis window, so deeper levels are not shown. Confidence intervals are wider relative to the signal than in Fig. 1 because cast clustering within cruises is stronger on the shelf, with variance inflation factors of 5.7–6.3 against 1.8–2.2 in the south.

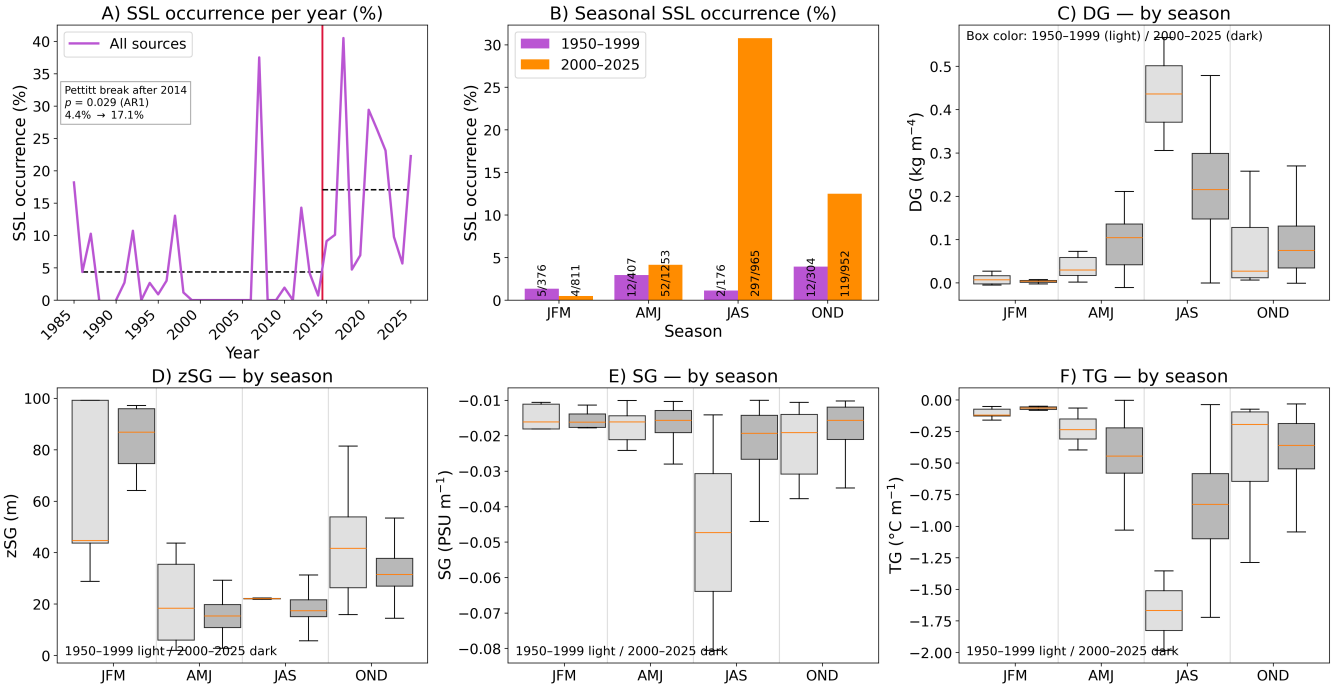


Figure 3. Surface saline lakes in the southern Adriatic, restricted to resolution-matched casts: median level spacing ≤ 5 m and at least 8 levels in 0–100 m, computed per cast from the source profiles. **(A)** Annual occurrence among evaluated casts; the red line marks the Pettitt test-derived regime shift after 2014 and the dashed lines the means either side. **(B)** Seasonal occurrence by period, annotated with detections over evaluated casts. **(C–F)** Seasonal distributions of the density gradient, core depth, salinity gradient and temperature gradient of the SSL core, for detected events only, light boxes for 1950–1999 and dark for 2000–2025. Restricting to matched casts is essential: at historical bottle spacing the detection criteria return nothing at all (Fig. A1). The 1950–1999 summer boxes in (C–F) rest on the two matched detections of that season and period (panel B) and should not be read as distributions.

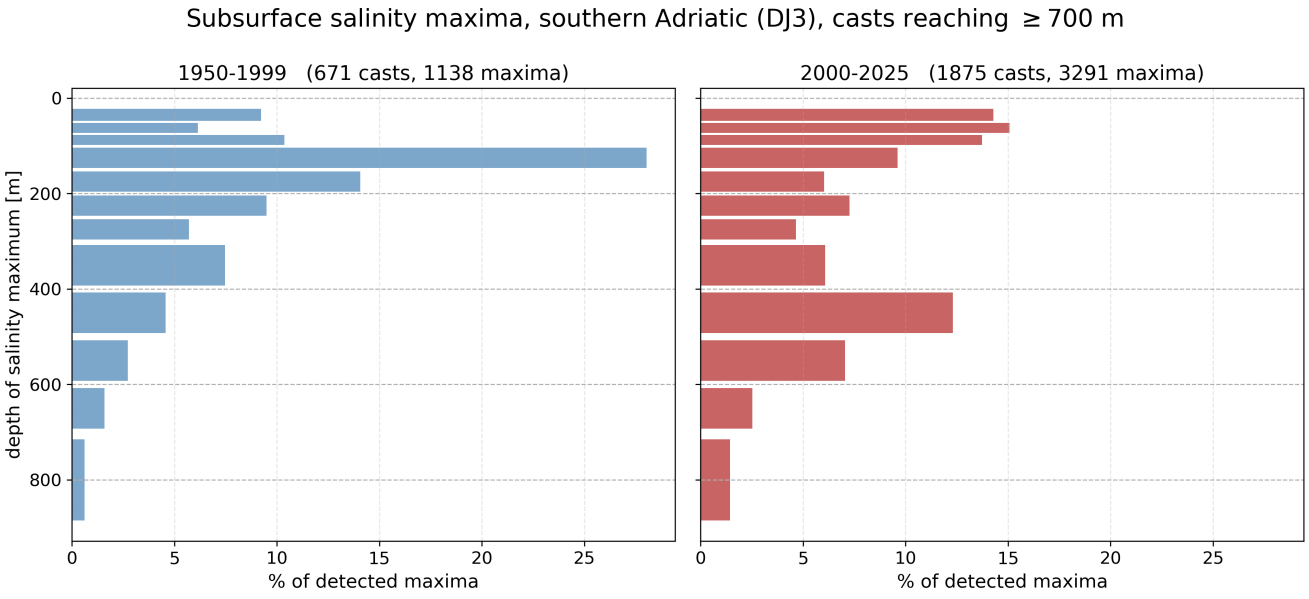


Figure 4. Subsurface salinity maxima in the southern Adriatic, detected individually in each cast by peak prominence, for 1950–1999 and 2000–2025. Only casts reaching 700 m are used, which alone can resolve both features, and only the two most prominent maxima of each cast are retained; a cast carrying a single maximum contributes one detection, which is why the number of maxima is less than twice the number of casts. The cap is needed because at a prominence threshold of 0.010 a small number of very high-resolution historical casts return hundreds of peaks each, and twenty such casts would otherwise supply more than half of all 1950–1999 detections. In 1950–1999 the maxima concentrate in one band, 28 % of them in the single 100–150 m interval and 42 % within 100–200 m; in 2000–2025 that band holds 16 % and the detections are spread through the column, both above 100 m and below 300 m. The historical distribution is what a single-core description of the intermediate layer represents; the modern one is not. Detection is on native vertical resolution; the degraded-resolution repeat is reported in Sect. 3.4. Panels share a common horizontal scale.

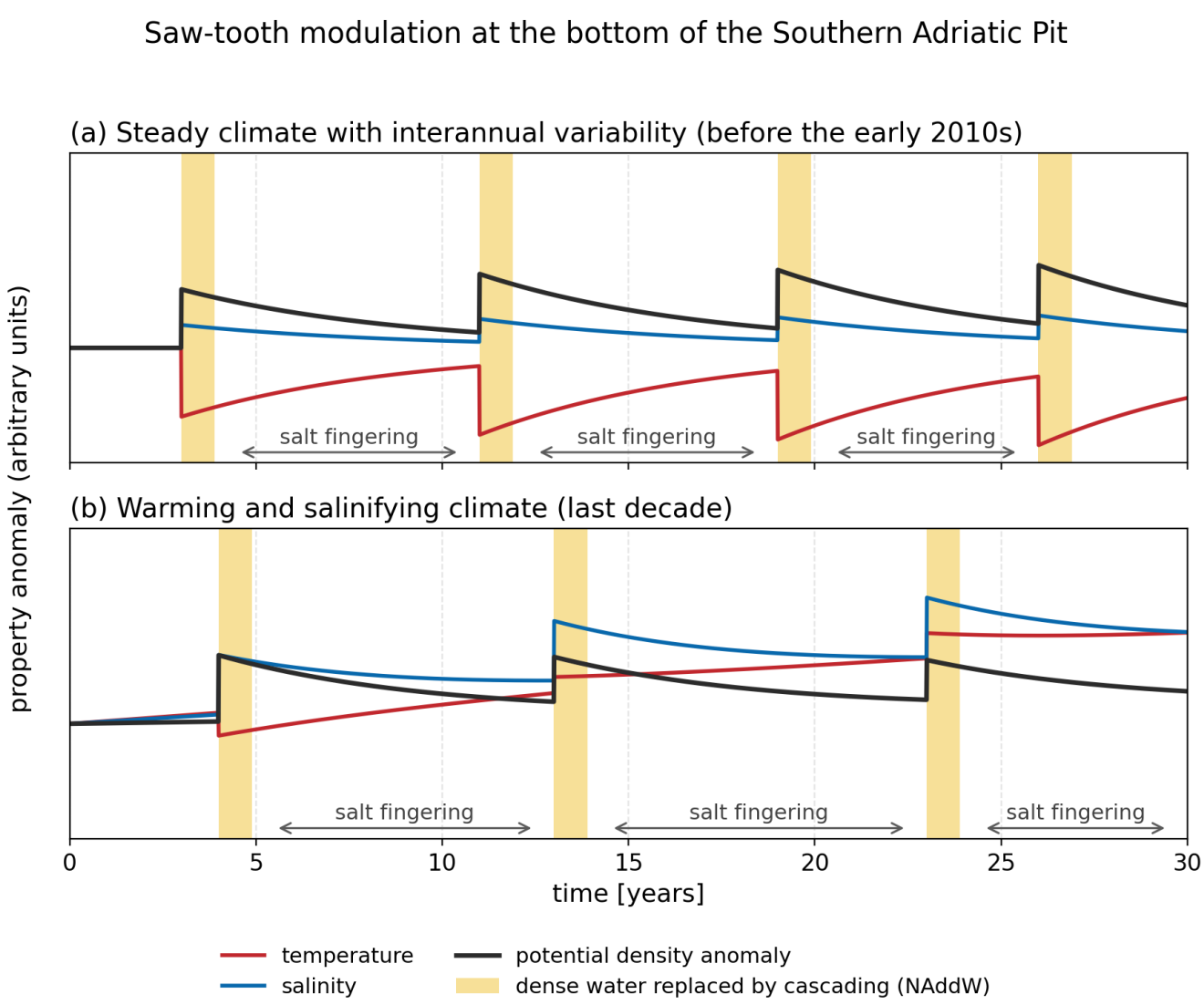


Figure 5. Schematic saw-tooth modulation of temperature, salinity and potential density anomaly at the bottom of the Southern Adriatic Pit. Panel (a) follows the saw-tooth described by Querin et al. (2016); panel (b) sketches how it is modified under the recent regime. **(a)** Steady climate with interannual variability, before the early 2010s: each cascading event delivers cold water, so density rises mainly through the thermal term and properties differ from year to year. **(b)** Warming and salinifying climate of the last decade (Terzić et al., 2025a): cascading water is only weakly cooled but much saltier, so the density step is smaller and the record carries an underlying warming and salinifying drift. The temperature step no longer has a fixed sign. The first event sketched here still cools the deep layer, while the later two bring water warmer than the water they replace, so an event can now raise deep temperature as well as lower it. Yellow bars mark the intervals during which resident deep water is replaced by cascading North Adriatic Dense Water; between them, properties relax under double-diffusive and other mixing. Salt fingering is marked over the relaxation phases only, and is intermittent because the density ratio rather than the Turner angle governs whether fingers transport appreciably (Sect. 3.7). This is a schematic, not a data plot.

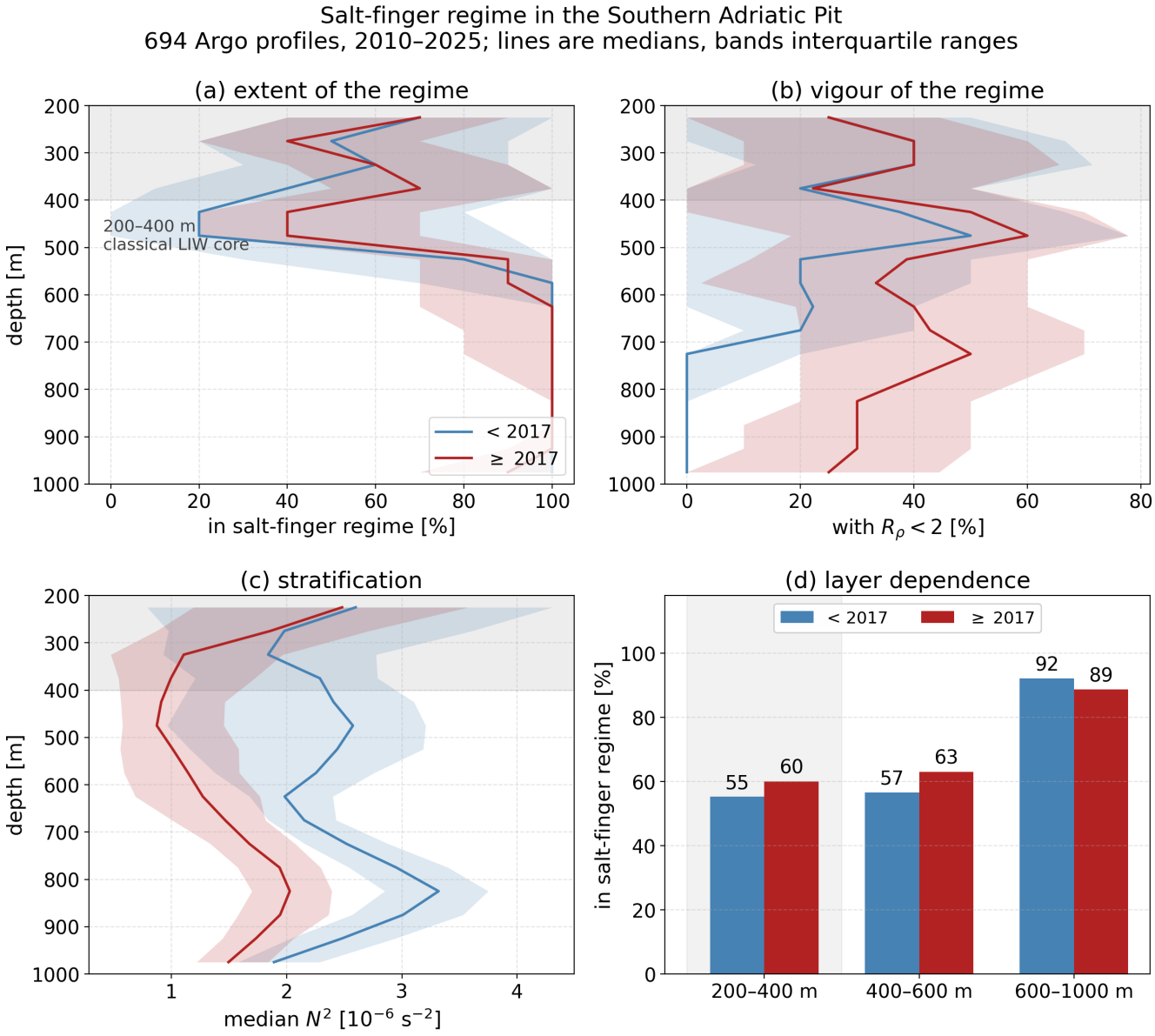


Figure 6. Salt-finger regime in the Southern Adriatic Pit from 694 Argo profiles, 2010–2025, split before and from 2017. Lines are medians across profiles within each 50 m depth bin, bands the interquartile range. **(a)** Fraction of each bin in the salt-finger regime: the extent of the regime. **(b)** Fraction with density ratio $R_\rho < 2$, the range in which fingers grow fast enough to outrun internal-wave strain: the vigour of the regime. **(c)** Median N^2. The grey band marks the classical 200–400 m LIW salinity-maximum range. **(d)** The three layers of Sect. 2.9 compared directly, as the extent of the regime before and from 2017: within the shaded core it does not change significantly (55 % against 60 %, $p = 0.07$), it rises below the core (57 % to 63 % at 400–600 m) and edges down in the deep layer (92 % to 89 %) where the regime is already close to saturation. The vigour of the regime, panel (b), separates the layers far more sharply than the extent does; both are tabulated with their p-values in Table 5.

Appendix A: Supporting analyses

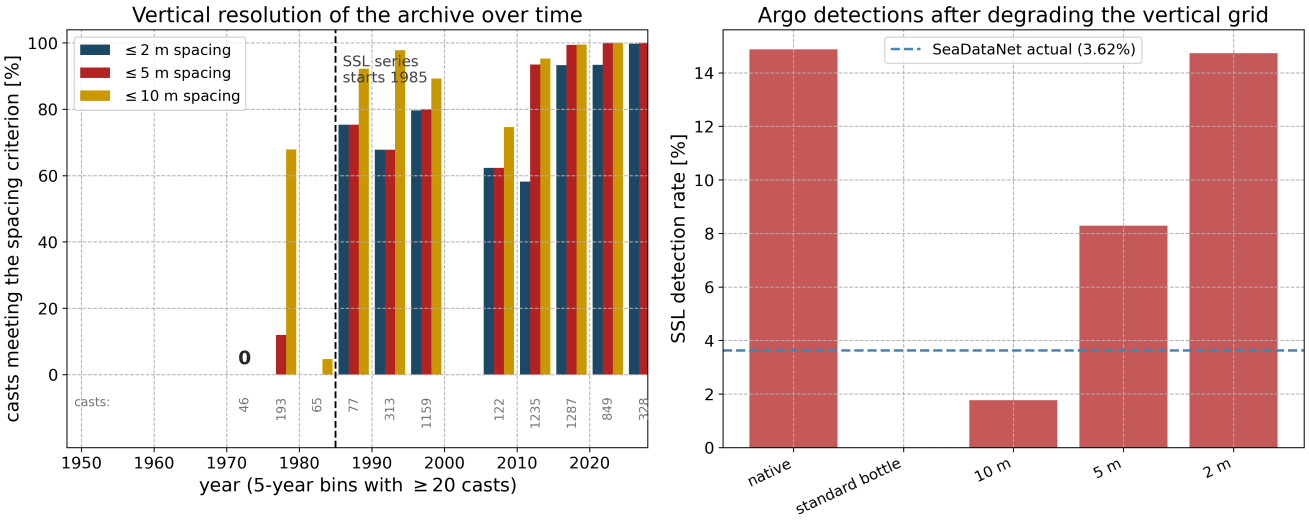


Figure A1. Why surface saline lake occurrence must be read on resolution-matched casts. **Left:** the vertical resolution of the southern Adriatic archive itself, as the percentage of casts per five-year bin whose median level spacing in 0–100 m meets each criterion; bins with fewer than 20 casts are omitted. Bins are labelled with the number of casts behind them, and a bin whose bars are all zero is marked "0", so that an empty bin is not read as missing data. Before 1975 casts exist but none reaches even 10 m median spacing; the 1975–1979 casts are markedly better, 68 % of them at 10 m and 12 % at 5 m, but those fine casts carry too few levels to be evaluated (Sect. 2.6), which is why occurrence is plotted only from 1985 (dashed line). After 2015 almost every cast meets the 5 m resolution threshold. **Right:** the degradation experiment. Argo profiles are re-sampled onto progressively coarser vertical grids and the identical detection criteria re-applied. Detections fall from 438 (14.87 %) at native 1–5 m spacing to 434 at 2 m, 244 at 5 m, 52 at 10 m and zero on the standard bottle grid (0, 10, 20, 30, 50, 75, 100 m), in profiles that demonstrably contain a surface saline lake at native resolution; the dashed line is the rate SeaDataNet actually returns at its own resolution. Together these are the justification for the resolution threshold applied in Fig. 3.

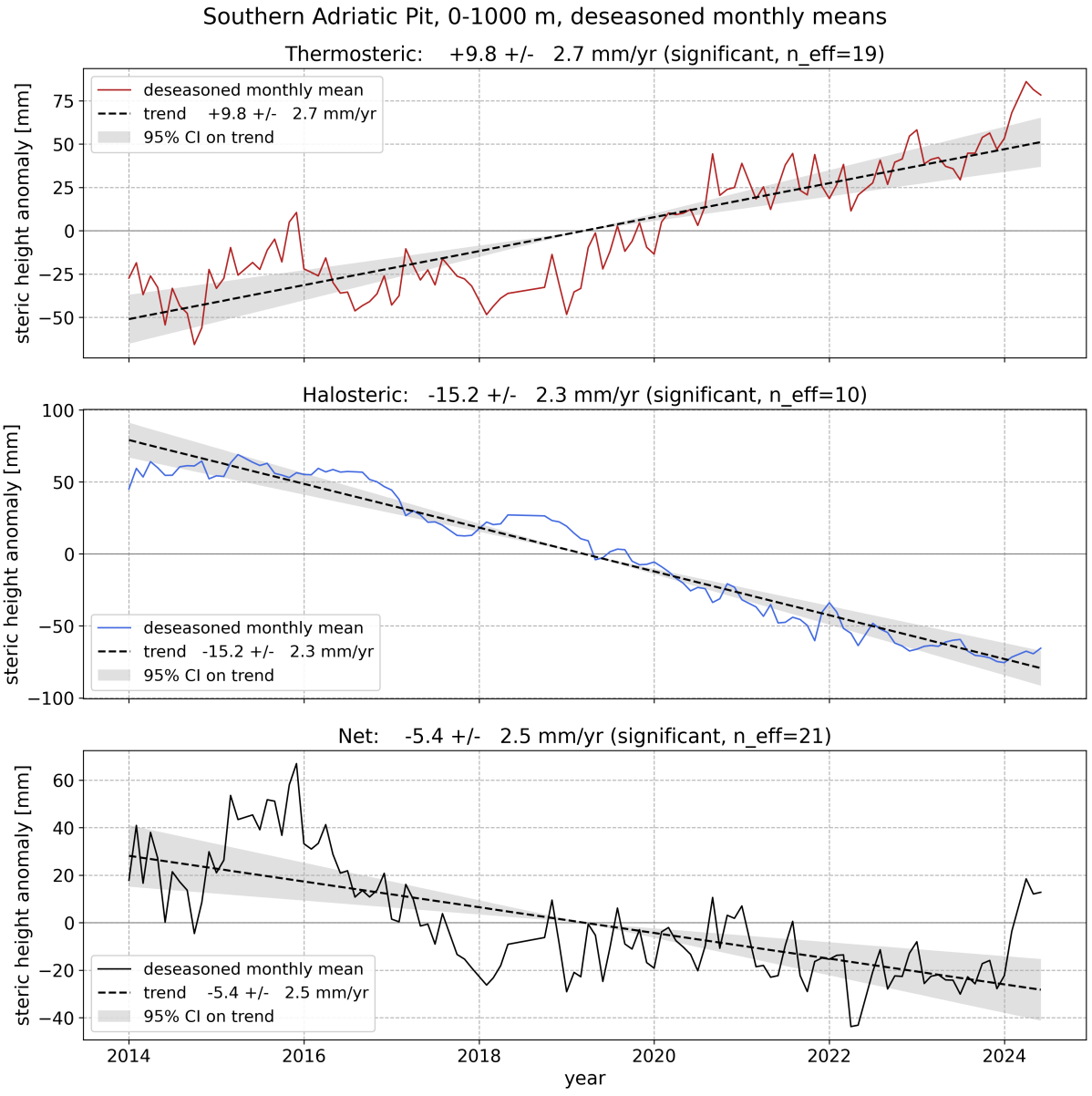


Figure A2. Thermosteric, halosteric and net steric height in the Southern Adriatic Pit over 2014–2024, the window of Table 3, from deseasoned monthly means on a common 0–1000 dbar grid, with fitted trends and 95 % confidence bands corrected for residual autocorrelation. Anomalies are shown about each series mean, so that the three panels are comparable. The window holds 121 monthly values, but successive months resemble one another (lag-1 correlation 0.7–0.8), so the effective sample size $n_{\mathrm{eff}} = n(1-r_1)/(1+r_1)$ behind each interval is only 10–21. The bands are wide for that reason, not because the monthly means are noisy.

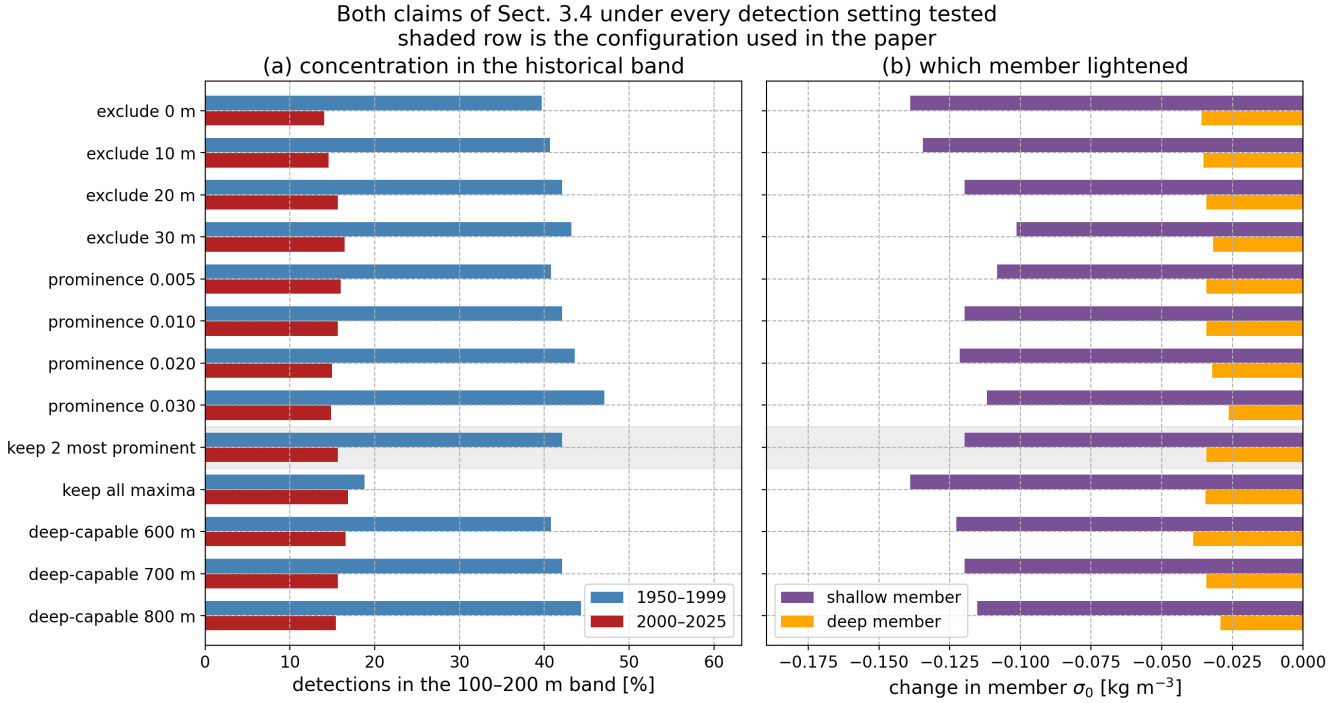


Figure A3. The two claims of Sect. 3.4 under every setting of the detection we tested. The free parameters (Sect. 2.7) are the depth above which maxima are ignored, the prominence threshold, whether all maxima or only the two most prominent are kept per cast, and how deep a cast must reach to be used; each row varies one of them and the shaded row is the configuration used in the paper. **(a)** Share of detected maxima falling in the 100–200 m band. It is higher in 1950–1999 than in 2000–2025 in all thirteen configurations, by 39.7–47.1 % against 14.0–16.9 %. **(b)** Change in σ_0 of each member between the periods. The shallower member lightens by three to four times as much as the deeper one, again in every configuration.